Inorg. Chem. **2005**, *44*, 7345–7364

Bis(μ-oxo)dicopper(III) Complexes of a Homologous Series of Simple Peralkylated 1,2-Diamines: Steric Modulation of Structure, Stability, and Reactivity

Adam P. Cole, Viswanath Mahadevan, Liviu M. Mirica, Xavier Ottenwaelder, and T. Daniel P. Stack*

Contribution from the Department of Chemistry, Stanford University, Stanford, California 94305

Received March 3, 2005

We have synthesized and characterized bis(μ-oxo)dicopper(III) dimers **1b**–**4b** (**O**s) based on a core family of peralkylated *trans*-(1*R*,2*R*)-cyclohexanediamine (CD) ligands, self-assembled from the corresponding [LCu(MeCN)]CF_3SO_3 species **1a**–**4a** and O_2 at 193 K in aprotic media; additional **O**s based on peralkylated ethylenediamine and tridentate polyazacyclononane ligands were synthesized analogously for comparative purposes (**5b**–**7b** and **8b**–**9b**, respectively). Trigonal-planar $[LCu(MeCN)]^{1+}$ species are proposed as the active **O** precursors. The 3-coordinate Cu(I) complexes [(**L**$^{\mathbf{TE}}$)Cu(MeCN)]CF_3SO_3 (**4a**) and [(**L**$^{\mathbf{TB}}$)Cu(MeCN)]CF_3SO_3 (**10a**) were structurally characterized; the apparent O_2-inertness of **10a** correlates with the steric demands of its four benzyl substituents. The rate of **O** formation, a multistep process that likely proceeds via associative formation of a 1:1 $[LCu(O_2)]^{1+}$ intermediate, exhibits significant dependence upon ligand sterics and solvent: oxygenation of **4a**—the slowest-reacting **O** precursor of the CD series—is first-order with respect to [**4a**] and proceeds at least 300 times faster in tetrahydrofuran than in CH_2Cl_2. The EPR, UV–vis, and resonance Raman spectra of **1b**–**9b** are all characteristic of the diamagnetic bis(μ-oxo)dicopper(III) core. The intense ligand-to-metal charge transfer absorption maxima of CD-based **O**s are red-shifted proportionally with increasing peripheral ligand bulk, an effect ascribed to a slight distortion of the $[Cu_2O_2]$ rhomb. The well-ordered crystal structure of [(**L**$^{\mathbf{ME}}$)$_2Cu_2(\mu\text{-}O)_2$]$(CF_3SO_3)_2\cdot 4CH_2Cl_2$ ([**3b**·$4CH_2Cl_2$]) features the most metrically compact $[Cu_2O_2]^{2+}$ core among structurally characterized **O**s (av Cu–O 1.802(7) Å; Cu···Cu 2.744(1) Å) and exemplifies the minimal square-planar ligation environment necessary for stabilization of Cu(III). The reported **O**s are mild oxidants with moderate reactivity toward coordinating substrates, readily oxidizing thiols, certain activated alkoxides, and electron-rich phenols in a net $2e^-$, $2H^+$ process. In the absence of substrates, **1b**–**9b** undergo thermally induced autolysis with concomitant degradation of the polyamine ligands. Ligand product distribution and primary kinetic isotope effects ($k_{obs}^H/k_{obs}^D \approx 8$, **1b**/$d_{24}$-**1b**, 293 K) support a unimolecular mechanism involving rate-determining C–H bond cleavage at accessible ligand *N*-alkyl substituents. Decomposition half-lives span almost 3 orders of magnitude at 293 K, ranging from ∼2 s for **4b** to almost 30 min for d_{24}-**1b**, the most thermally robust dicationic **O** yet reported. Dealkylation is highly selective where ligand rigidity constrains accessibility; in **3b**, the ethyl groups are attacked preferentially. The observed relative thermal stabilities and dealkylation selectivities of **1b**–**9b** are correlated with NC^{α}–H bond dissociation energies, statistical factors, ligand backbone rigidity, and ligand denticity/axial donor strength. Among the peralkylated amines surveyed, bidentate ligands with oxidatively robust NC^{α}–H bonds provide optimal stabilization for **O**s. Fortuitously, the least sterically demanding *N*-alkyl substituent (methyl) gives rise to the most thermally stable and most physically accessible **O** core, retaining the potential for exogenous substrate reactivity.

Introduction

The bis(μ-oxo)dicopper(III) dimer is one of several recurring structural motifs in $Cu-O_2$ chemistry, an area of relevance to metallobiology and synthetic oxidative catalysis that has attracted strong interest over the past two decades.[1−12] Recent work has probed the relationship between the structure and function of natural $Cu-O_2$ species, as well as synthetic model systems, further contributing to a wealth of

* To whom correspondence should be addressed. E-mail: stack@stanford.edu.

10.1021/ic050331i CCC: $30.25
Published on Web 09/21/2005

structural, spectroscopic, and mechanistic data concerning their formation and reactivity.[1,2] Synthetic binuclear Cu−O_2 systems have frequently employed tridentate aromatic or aliphatic nitrogen ligands in emulation of natural biochemical environments such as that of hemocyanin (Hc), in which each Cu is ligated by three histidine residues in both the oxygenated and the reduced forms.[13] Yet, in oxyHc and all other structurally characterized Cu−O_2 complexes that comprise such tridentate amine ligands, the third, axially disposed N donor is but weakly bound to Cu.[13−20] A marked preference for square-planar coordination dominates the chemistry of trivalent Cu and forms the basis for an emerging trend in which sterically demanding *bidentate* nitrogen ligands are used to stabilize bis(μ-oxo)dicopper(III) (**O**)[21−33] and μ-η^2:η^2-peroxodicopper(II) (**P**)[34] dimers, as well as interconverting mixtures thereof.[35]

Simple aliphatic diamines constitute a vast and versatile pool of inexpensive, easily modified bidentate ligands. Yet, despite their well-known empirical use in conjunction with Cu salts and atmospheric O_2 for various "one-pot" oxidative transformations involving unknown active species,[36,37] they have been largely ignored in the context of designing ligands to support Cu−O_2 intermediates. In 1984, Thompson did report a putative Cu(II)−peroxo species, obtained by reacting $[(\mathbf{L}^{\mathbf{TEED}})\mathrm{Cu}]^{1+}$ ($\mathbf{L}^{\mathbf{TEED}}$ = *N*,*N*,*N*′,*N*′-tetraethyl-1,2-ethanediamine) with O_2 at 193 K in wet methanol (MeOH).[38,39] The adduct is stable in the solid state at room temperature but readily decomposes in solution via hydroxylation of the ligand. Encouraged by this result and by the general synthetic flexibility afforded by *N*-peralkylated diamine ligands (PDLs), we systematically explored the low-temperature O_2 reactivity of a series of Cu(I)−PDL complexes in aprotic solvents with weakly coordinating counteranions.[40] In several instances, a new Cu−O_2 species with spectroscopic features distinct from those of any Cu−O_2 complex then known was observed.[41,42] One set of such features is now diagnostic for **O**s, and numerous spectroscopically and/or structurally characterized examples have since been reported.[8,16,17,21−33,35,43−53]

(1) Mirica, L. M.; Ottenwaelder, X.; Stack, T. D. P. *Chem. Rev.* **2004**, *104*, 1013−1045.
(2) Lewis, E. A.; Tolman, W. B. *Chem. Rev.* **2004**, *104*, 1047−1076.
(3) Karlin, K. D.; Tyeklár, Z., Eds. *Bioinorganic Chemistry of Copper*; Chapman and Hall: New York, 1993.
(4) Barton, D. H. R.; Martell, A. E.; Sawyer, D. T. *The Activation of Dioxygen and Homogeneous Catalysis*; Plenum Press: New York, 1993.
(5) Kitajima, N.; Moro-Oka, Y. *Chem. Rev.* **1994**, *94*, 737−757.
(6) Fox, S.; Karlin, K. D. In *Active Oxygen in Biochemistry*; Valentine, J. S., Foote, C. S., Greenberg, A., Liebman, J. F., Eds.; Blackie Academic and Professional: London, 1995; pp 188−231.
(7) Solomon, E. I.; Sundaram, U. M.; Machonkin, T. E. *Chem. Rev.* **1996**, *96*, 2563−2606.
(8) Tolman, W. B. *Acc. Chem. Res.* **1997**, *30*, 227−237.
(9) Blackman, A. G.; Tolman, W. B. *Struct. Bond.* **2000**, *97*, 179−211.
(10) Schindler, S. *Eur. J. Inorg. Chem.* **2000**, 2311−2326.
(11) Mahadevan, V.; Klein Gebbink, R. J. M.; Stack, T. D. P. *Curr. Opin. Chem. Biol.* **2000**, *4*, 228−234.
(12) Solomon, E. I.; Chen, P.; Metz, M.; Lee, S.-K.; Palmer, A. E. *Angew. Chem., Int. Ed.* **2001**, *40*, 4570−4590.
(13) Magnus, K. A.; Hazes, B.; Ton-That, H.; Bonaventura, C.; Bonaventura, J.; Hol, W. G. J. *Proteins: Struct., Funct., Genet.* **1994**, *19*, 302−309.
(14) Kitajima, N.; Fujisawa, K.; Moro-Oka, Y.; Toriumi, K. *J. Am. Chem. Soc.* **1989**, *111*, 8975−8976.
(15) Fujisawa, K.; Tanaka, M.; Moro-Oka, Y.; Kitajima, N. *J. Am. Chem. Soc.* **1994**, *116*, 12079−12080.
(16) Mahapatra, S.; Halfen, J. A.; Wilkinson, E. C.; Pan, G. F.; Wang, X. D.; Young, V. G.; Cramer, C. J.; Que, L., Jr.; Tolman, W. B. *J. Am. Chem. Soc.* **1996**, *118*, 11555−11574.
(17) Mahapatra, S.; Young, V. G.; Kaderli, S.; Zuberbühler, A. D.; Tolman, W. B. *Angew. Chem., Int. Ed. Engl.* **1997**, *36*, 130−133.
(18) Pidcock, E.; Debeer, S.; Obias, H. V.; Hedman, B.; Hodgson, K. O.; Karlin, K. D.; Solomon, E. I. *J. Am. Chem. Soc.* **1999**, *121*, 1870−1878.
(19) Kodera, M.; Katayama, K.; Tachi, Y.; Kano, K.; Hirota, S.; Fujinami, S.; Suzuki, M. *J. Am. Chem. Soc.* **1999**, *121*, 11006−11007.
(20) Kodera, M.; Kajita, Y.; Tachi, Y.; Katayama, K.; Kano, K.; Hirota, S.; Fujinami, S.; Suzuki, M. *Angew. Chem., Int. Ed.* **2004**, *43*, 334−337.
(21) Mahadevan, V.; Hou, Z. G.; Cole, A. P.; Root, D. E.; Lal, T. K.; Solomon, E. I.; Stack, T. D. P. *J. Am. Chem. Soc.* **1997**, *119*, 11996−11997.
(22) Mahadevan, V.; Dubois, J. L.; Hedman, B.; Hodgson, K. O.; Stack, T. D. P. *J. Am. Chem. Soc.* **1999**, *121*, 5583−5584.
(23) Holland, P. L.; Rodgers, K. R.; Tolman, W. B. *Angew. Chem., Int. Ed.* **1999**, *38*, 1139−1142.
(24) Itoh, S.; Taki, M.; Nakao, H.; Holland, P. L.; Tolman, W. B.; Que, L., Jr.; Fukuzumi, S. *Angew. Chem., Int. Ed.* **2000**, *39*, 398−400.
(25) Funahashi, Y.; Nakaya, K.; Hirota, S.; Yamauchi, O. *Chem. Lett.* **2000**, 1172−1173.
(26) Holland, P. L.; Cramer, C. J.; Wilkinson, E. C.; Mahapatra, S.; Rodgers, K. R.; Itoh, S.; Taki, M.; Fukuzumi, S.; Que, L.; Tolman, W. B. *J. Am. Chem. Soc.* **2000**, *122*, 792−802.
(27) Straub, B. F.; Rominger, F.; Hofmann, P. *Chem. Commun.* **2000**, 1611−1612.
(28) Taki, M.; Itoh, S.; Fukuzumi, S. *J. Am. Chem. Soc.* **2001**, *123*, 6203−6204.
(29) Taki, M.; Itoh, S.; Fukuzumi, S. *J. Am. Chem. Soc.* **2002**, *124*, 998−1002.
(30) Taki, M.; Teramae, S.; Nagatomo, S.; Tachi, Y.; Kitagawa, T.; Itoh, S.; Fukuzumi, S. *J. Am. Chem. Soc.* **2002**, *124*, 6367−6377.
(31) Spencer, D. J. E.; Aboelella, N. W.; Reynolds, A. M.; Holland, P. L.; Tolman, W. B. *J. Am. Chem. Soc.* **2002**, *124*, 2108−2109.
(32) Aboelella, N. W.; Lewis, E. A.; Reynolds, A. M.; Brennessel, W. W.; Cramer, C. J.; Tolman, W. B. *J. Am. Chem. Soc.* **2002**, *124*, 10660−10661.
(33) Spencer, D. J. E.; Reynolds, A. M.; Holland, P. L.; Jazdzewski, B. A.; Duboc-Toia, C.; Le Pape, L.; Yokota, S.; Tachi, Y.; Itoh, S.; Tolman, W. B. *Inorg. Chem.* **2002**, *41*, 6307−6321.
(34) Mirica, L. M.; Vance, M.; Rudd Jackson, D.; Hedman, B.; Hodgson, K. O.; Solomon, E. I.; Stack, T. D. P. *J. Am. Chem. Soc.* **2002**, *124*, 9332−9333.
(35) Mahadevan, V.; Henson, M. J.; Solomon, E. I.; Stack, T. D. P. *J. Am. Chem. Soc.* **2000**, *122*, 10249−10250.
(36) Aycock, D.; Abolins, V.; White, D. M. *Encyclopedia of Polymer Science and Engineering*, 2nd ed.; John Wiley and Sons: New York, 1986; Vol. 13.
(37) Oyaizu, K.; Saito, K.; Tsuchida, E. *Chem. Lett.* **2000**, 1318−1319.
(38) Thompson, J. S. *J. Am. Chem. Soc.* **1984**, *106*, 8308−8309.
(39) Thompson, J. S. In *Biological and Inorganic Copper Chemistry*; Karlin, K. D., Zubieta, J., Eds.; Adenine Press: Guilderland, NY, 1986.
(40) Stack, T. D. P. *Dalton Trans.* **2003**, *10*, 1881−1889.
(41) Mahapatra, S.; Halfen, J.; Wilkinson, E.; Pan, G.; Cramer, C. J.; Que, L., Jr.; Tolman, W. B. *J. Am. Chem. Soc.* **1995**, *117*, 8865−8866.
(42) Cole, A. P.; Root, D. E.; Mukherjee, P.; Solomon, E. I.; Stack, T. D. P. *Science* **1996**, *273*, 1848−1850.
(43) Mahapatra, S.; Kadereli, S.; Llobet, A.; Neuhold, Y. M.; Palanche, T.; Halfen, J. A.; Young, V. G.; Kaden, T. A.; Que, L.; Zuberbühler, A. D.; Tolman, W. B. *Inorg. Chem.* **1997**, *36*, 6343−6356.
(44) Halfen, J. A.; Mahapatra, S.; Wilkinson, E. C.; Kaderli, S.; Young, V. G.; Que, L., Jr.; Zuberbühler, A. D.; Tolman, W. B. *Science* **1996**, *271*, 1397−1400.
(45) Mahapatra, S.; Halfen, J. A.; Tolman, W. B. *J. Am. Chem. Soc.* **1996**, *118*, 11575−11586.
(46) Lam, B. M. T.; Halfen, J. A.; Young, V. G.; Hagadorn, J. R.; Holland, P. L.; Lledós, A.; Cucurull-Sánchez, L.; Novoa, J. J.; Alvarez, S.; Tolman, W. B. *Inorg. Chem.* **2000**, *39*, 4059−4072.
(47) Liang, H.-C.; Zhang, C. X.; Henson, M. J.; Sommer, R. D.; Hatwell, K. R.; Kaderli, S.; Zuberbühler, A. D.; Rheingold, A. L.; Solomon, E. I.; Karlin, K. D. *J. Am. Chem. Soc.* **2002**, *124*, 4170−4171.
(48) Uozumi, K.; Hayashi, Y.; Suzuki, M.; Uehara, A. *Chem. Lett.* **1993**, 963−966.
(49) Hayashi, H.; Fujinami, S.; Nagatomo, S.; Ogo, S.; Suzuki, M.; Uehara, A.; Watanabe, Y.; Kitagawa, T. *J. Am. Chem. Soc.* **2000**, *122*, 2124−2125.

Table 1. Nomenclature of Ligands and Cu Complexes

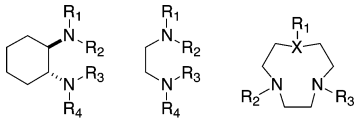

ligand	type	R_1	R_2	R_3	R_4	Cu(I)[a,b]	O[b,c]
$\mathbf{L^{TM}}$	CD	Me	Me	Me	Me	**1a**	**1b**
$\mathbf{L^{EtMe_3}}$	CD	Et	Me	Me	Me	**2a**	**2b**
$\mathbf{L^{ME}}$	CD	Et	Me	Et	Me	**3a**	**3b**
$\mathbf{L^{TE}}$	CD	Et	Et	Et	Et	**4a**	**4b**
$\mathbf{L^{TEED}}$	ED	Et	Et	Et	Et	**5a**	**5b**
$\mathbf{L^{(MeEt)_2ED}}$	ED	Et	Me	Et	Me	**6a**	**6b**
$\mathbf{L^{Me_2Et_2ED}}$	ED	Me	Me	Et	Et	**7a**	**7b**
$\mathbf{L^{Me_3TACN}}$ (X = N)	[9]ane	Me	Me	Me	−	**8a**	**8b**
$\mathbf{L^{Me_2ODACN}}$ (X = O)	[9]ane	−	Me	Me	−	**9a**	**9b**
$\mathbf{L^{TB}}$	CD	Bz	Bz	Bz	Bz	**10a**	−

[a] **Cu(I)** = $[LCu(MeCN)]^{1+}$. [b] $CF_3SO_3^-$ counteranion assumed unless stated otherwise. [c] **O** = $[L_2Cu_2(\mu\text{-}O)_2]^{2+}$.

Extensive study of almost 20 such **O**s generated from a broad range of PDLs has helped define the general structural, spectroscopic, and reactive character of these complexes. We take particular interest in ligand structural attributes that determine the products and mechanism of thermal decay for each **O**, as these provide an intrinsic failure analysis for ligand design. Developing improved ligands that support more thermally stable **O**s will require a firm understanding of these factors. Such stability, often viewed as an end in itself, is also a prerequisite to designing a useful reagent capable of directing its oxidizing capacity beyond its own ligands to exogenous substrates. A more thermally robust oxidant will provide access to substrate oxidation processes with much larger activation barriers.

This article confines itself to the discussion and comparison of seven **O**s generated from a series of related PDLs based on the *trans*-(1*R*,2*R*)-cyclohexanediamine (CD) and 1,2-ethanediamine (ED) skeletons, as well as two tridentate **O**s based on polyazacyclononane ([9]ane) ligands. Although much of the data presented in depth is derived from compounds representative of the first group, the general arguments herein apply to all **O**s studied unless otherwise indicated. Selected **O**s are also synoptically compared with other reported $[Cu_2(\mu\text{-}O)_2]^{2+}$ species.

Results

Ligand Syntheses. All ligand syntheses involved routine direct *N*-peralkylation or *N*-acylation followed by reduction and further alkylation; ligand nomenclature is given in Table 1. CD-based PDLs (Scheme 1) were synthesized as the pure 1*R*,2*R* enantiomers ($_{RR}\mathbf{L^X}$, abbreviated $\mathbf{L^X}$) unless otherwise specified ($_{SS}\mathbf{L^X}$ or $_{rac}\mathbf{L^X}$). Tridentate facial-capping [9]ane

Scheme 1. Synthesis of a Family of Peralkylated Enantiopure $_{RR}$CD Ligands

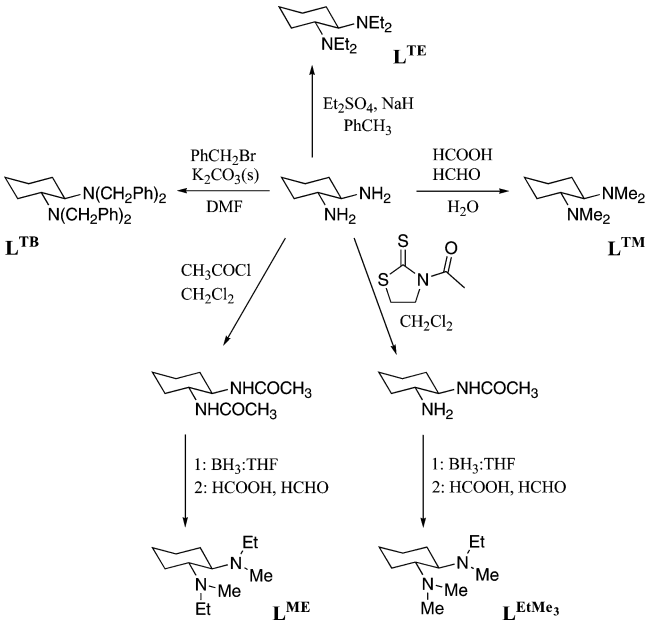

ligands $\mathbf{L^{Me_3TACN}}$ and $\mathbf{L^{Me_2ODACN}}$ were prepared according to literature methods.[54−56] The bidentate ligands $\mathbf{L^{TM}}$, $_{rac}\mathbf{L^{TM}}$, $\mathbf{L^{ME}}$, $\mathbf{L^{EtMe_3}}$, $\mathbf{L^{TE}}$, and $\mathbf{L^{TB}}$ were synthesized by peralkylation of enantiopure CD or its racemate $_{rac}$CD (Scheme 1); $\mathbf{L^{TEED}}$ and the substitution isomers $\mathbf{L^{Me_2Et_2ED}}$ (nonsymmetric) and $\mathbf{L^{(MeEt)_2ED}}$ (symmetric) were either purchased or obtained through analogous manipulation of ED. Only the nonsymmetrically substituted $\mathbf{L^{EtMe_3}}$ presented a potential synthetic challenge. The desired substituent pattern was introduced via a modified procedure for *N*-acylation popularized by Nagao[57,58] in which a 3-acyl-1,3-thiazolidine-2-thione ester is substituted for the traditional acyl chloride. This milder reagent affords better selectivity and greater yield of the *N*-monoacetylated derivative, which is conveniently isolated and purified through sublimation. Subsequent reduction and permethylation of this key intermediate were accomplished in a routine manner.

Mononuclear Cu(I) Precursor Complexes. Mononuclear Cu(I) complexes **1a**−**10a** having the general formula $[LCu(MeCN)]CF_3SO_3$ (Table 1) were synthesized by equimolar admixture of $[Cu(MeCN)_4]CF_3SO_3$ with ligand in purified, anhydrous solvent (CH_2Cl_2, unless otherwise stated) in a N_2 drybox. With the exception of **2a** and **7a**, which contain nonsymmetric ligands, the ^{1}H NMR spectra of the CD- and ED-based 1:1 Cu(I) complexes reflect overall C_2 molecular symmetry. When **1a**−**10a** are prepared in situ (i.e., in the presence of 3 equiv of excess MeCN), their ^{1}H NMR spectra contain only a single resonance due to MeCN at δ = 2.05−

(50) Hayashi, H.; Uozumi, K.; Fujinami, S.; Nagatomo, S.; Shiren, K.; Furutachi, H.; Suzuki, M.; Uehara, A.; Kitagawa, T. *Chem. Lett.* **2002**, 416−417.
(51) Mizuno, M.; Hayashi, H.; Fujinami, S.; Furutachi, H.; Nagatomo, S.; Otake, S.; Uozumi, K.; Suzuki, M.; Kitagawa, T. *Inorg. Chem.* **2003**, *42*, 8534−8544.
(52) Berreau, L. M.; Halfen, J. A.; Young, V. G.; Tolman, W. B. *Inorg. Chim. Acta* **2000**, *297*, 115−128.
(53) Enomoto, M.; Aida, T. *J. Am. Chem. Soc.* **1999**, *121*, 874−875.
(54) Wieghardt, K.; Chaudhuri, P.; Nuber, B.; Weiss, J. *Inorg. Chem.* **1982**, *21*, 3086−3090.
(55) Reinen, D.; Ozarowski, A.; Jakob, B.; Pebler, J.; Stratemeier, H.; Wieghardt, K.; Tolksdorf, I. *Inorg. Chem.* **1987**, *26*, 4010−4017.
(56) Benson, S.; Cai, P.; Colon, M.; Haiza, M.; Tokles, M.; Snyder, J. *J. Org. Chem.* **1988**, *53*, 5335−5341.
(57) Nagao, Y.; Miyasaka, T.; Seno, K.; Yagi, M.; Fujita, E. *Chem. Lett.* **1981**, *4*, 463−466.
(58) Nagao, Y.; Seno, K.; Miyasaka, T.; Fujita, E. *Chem. Lett.* **1980**, 159−162.

Table 2. Crystal Data and Experimental Parameters for Structurally Characterized Compounds

	1c	**1d**	*RR,RR*-**1e**	*RR,SS*-**1e**	[**3b**·4CH_2Cl_2]	**4a**	[**10a**·2CH_2Cl_2]
formula	$CuSF_3O_3N_4C_{21}H_{44}$	$CuC_{29}H_{37}N_2PSO_3F_3$	$Cu_2N_4O_8F_6S_2C_{22}H_{46}$	$Cu_2N_4O_8F_6S_2C_{22}H_{46}$	$Cu_2S_2Cl_8F_6O_8N_4C_{30}H_{60}$	$CuC_{17}H_{33}F_3N_3O_3S_3$	$CuC_{38}H_{43}Cl_2F_3N_3O_3S$
fw (g mol^{-1})	553.21	645.20	799.83	799.83	1193.65	480.07	813.28
diffractometer	SMART CCD	CAD4	CAD4	CAD4	SMART CCD	CAD4	SMART CCD
T (K)	176(3)	203(1)	203(1)	203(1)	143(1)	203(1)	159(1)
lattice type	orthorhombic P	triclinic P	monoclinic P	orthorhombic P	monoclinic P	monoclinic P	monoclinic P
space group	$P2_12_12_1$ (no. 19)	$P\bar{1}$ (no. 1)	$P2_1$ (no. 4)	$Pbca$ (no. 61)	$P2_1$ (no. 4)	$P2_1$ (no. 4)	$P2_1$ (no. 4)
a (Å)	14.5032(3)	8.141(1)	13.770(2)	8.35(1)	12.1336(2)	10.127(1)	9.3741(2)
b (Å)	14.5032(3)	9.017(1)	8.508(1)	15.53(1)	11.9387(3)	8.290(1)	36.4647(7)
c (Å)	25.298(1)	12.239(1)	15.258(1)	26.16(2)	18.4717(3)	13.980(1)	11.3652(3)
α (°)	90	68.490(7)	90	90	90	90	90
β (°)	90	74.858(5)	108.212(8)	90	108.387(1)	105.52(1)	93.314(1)
γ (°)	90	67.016(7)	90	90	90	90	90
V (Å^3)	5321.3(2)	762.1(2)	1697.9(3)	3392(5)	2539.19(8)	1130.9(2)	3878.3(2)
Z	8	1	2	4	2	2	4
μ_{calc} (mm^{-1})	0.86	0.89	1.46	1.46	1.41	1.10	0.809
F_{000}	2352	336	828	1656	1224	504	1688
d_{calc} [d_{obs}[a]] (g cm^{-3})	1.381 [1.39]	1.41 [1.40]	1.56 [1.56]	1.57 [1.55]	1.56 [not measured]	1.41 [1.41]	1.39 [1.40]
size (mm^3)	0.35 × 0.32 × 0.25	0.50 × 0.30 × 0.30	0.40 × 0.30 × 0.20	0.40 × 0.20 × 0.20	0.20 × 0.10 × 0.10	0.50 × 0.20 × 0.20	0.42 × 0.35 × 0.20
scan width ω (°)	0.3	0.57 + 0.56 tan θ	0.66 + 0.84 tan θ	0.72 + 0.75 tan θ	0.3	0.57 + 0.56 tan θ	0.3
scan rate	10s exposure	5.5° min^{-1} in ω	5.4° min^{-1} in ω	8.2° min^{-1} in ω	10s exposure	5.5° min^{-1} in ω	20s exposure
max 2θ (°)	52.1	50.0	44.9	39.2	47.3	50.0	51.6
indexing reflns	9999	22	22	9	6569	25	5512
total reflns	25,668	2862	2495	1756	10,340	2222	18 537
unique reflns	9340	2862	2388	1485	6446	2128	10 975
obsd. reflns[b]	7354	2811	1974	925	5722	1834	9240
R_{int}	0.059	0.035	0.027	n/a	0.047	0.051	0.030
LS parameters	612	363	397	203	550	258	919
N_o/N_v[c]	15.26	7.89	6.02	7.32	11.72	8.25	11.94
R_1 [wR_2][d]	0.052 [0.112]	0.028 [0.076]	0.053 [0.150]	0.061 [0.188]	0.055 [0.129]	0.040 [0.109]	0.036 [0.071]
GOF, S[e]	0.98	1.07	1.07	1.04	1.08	1.04	1.00
LS weights m [n][f]	0.0504 [0.00]	0.0542 [0.2208]	0.0856 [4.050]	0.1046 [10.25]	0.0137 [10.5184]	0.0644 [0.5900]	0.0203 [0.00]
ρ_{max} [ρ_{min}] (e$^-$ Å^{-3})	0.93 [−0.66]	0.43 [−0.47]	0.89 [−0.49]	0.53 [−0.36]	0.88 [−0.71]	0.43 [−0.60]	0.24 [−0.29]

[a] Determined by the neutral buoyancy method in CCl_4/hexane. [b] $F_o > 4\sigma(F_o)$. [c] Reflection-to-parameter ratio. [d] $R_1 = \Sigma\ ||F_o| - |F_c||/\Sigma\ |F_o|$ based on observations with $F_o > 4\sigma(F_o)$; $wR_2 = [(\Sigma\ w(F_o^2 - F_c^2)^2/\Sigma\ wF_o^2)]^{1/2}$ based on all observations. [e] S = standard deviation of an observation of unit weight, or $[\Sigma\ w(F_o^2 - F_c^2)^2/(N_o - N_v)]^{1/2}$, where N_o = number of observations and N_v = number of variables. [f] The least-squares function minimized is $\Sigma\ w(F_o^2 - F_c^2)^2$, where $w = [\sigma^2(F_o^2) + (mP)^2 + nP]^{-1}$ and $P = [\mathrm{Max}\{F_o^2, 0\} + 2\ F_c^2]/3$.

2.20, even at 193 K; no distinct resonance corresponding to coordinated MeCN is observed. When samples of **4a** and **10a** are prepared from isolated solid, however, their spectra exhibit a sharp singlet resonance at $\delta \approx 2.15$ corresponding to one molecule of MeCN. We conclude that the auxiliary MeCN ligand in each of these in situ-prepared Cu(I) complexes undergoes facile exchange on the NMR time scale. In notable contrast to the other CD- and ED-based Cu(I) complexes, the ^{1}H NMR spectrum of the ED-based **5a** exhibits only an averaged singlet resonance corresponding to the backbone methylenes, even at 193 K. This observation reflects the flexibility of the ED ligand backbone in conjunction with the flat conformational potential energy profile due to the four identical *N*-ethyl substituents.

Crystal Structures of 1:1 Cu(I) Species. The 1:1 L/Cu(I) complexes **1a**−**10a** were generally prepared in situ and used in further experiments without isolation or purification; however, suitable single crystals of [(**L**$^{\mathbf{TE}}$)Cu(MeCN)]CF_3SO_3 (**4a**) and [(**L**$^{\mathbf{TB}}$)Cu(MeCN)]CF_3SO_3 (**10a**) were isolated and structurally characterized. In the solid-state structure of **4a** (Figure 1, Table 2), the Cu atom is 3-coordinate and is ligated in an approximately trigonal-planar fashion, the third coordination site being occupied by the MeCN molecule. The N−Cu−N bond angles deviate from the ideal trigonal-planar value of 120° because of the constrained 88° bite angle of the **L**$^{\mathbf{TE}}$ ligand.

The asymmetric unit of the [**10a**·2CH_2Cl_2] crystal structure (Figure 2 and Table 2) comprises two crystallographically

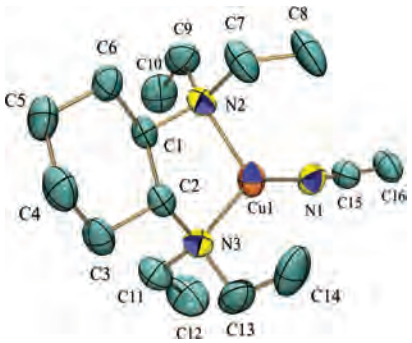

Figure 1. ORTEP representation (50% probability) of the monocation of **4a**, excluding hydrogen atoms. Selected interatomic distances (Å) and angles (deg): Cu(1)−N(1), 1.864(4); Cu(1)−N(2), 2.082(4); Cu(1)−N(3), 2.047(4); N(1)−C(15), 1.130(6); N(1)Cu(1)N(2), 130.2(2); N(1)Cu(1)N(3), 141.7(2); N(2)Cu(1)N(3), 88.1(2); Cu(1)N(1)C(15), 174.7(4).

independent monocations that are isostructural to within 0.346 Å rms as a whole and to within 0.078 Å rms excluding phenyl ring carbons. As in **4a**, the approximately trigonal-planar geometry about each 3-coordinate Cu atom is distorted from the ideal as a result of the ∼89° bite angle of the **L**$^{\mathbf{TB}}$ ligand. The relative orientations of the *N*-benzyl substituents within each cation are indicative of pairwise edge-to-face π-stacking interactions: the ortho protons of one monocation (on C43 and C47, Figure 2) and those of the other (on C32 and C48)[59] reside at distances of 2.59, 2.67, 2.59, and 2.50 Å, respectively, from the corresponding least-squares planes

(59) See Supporting Information.

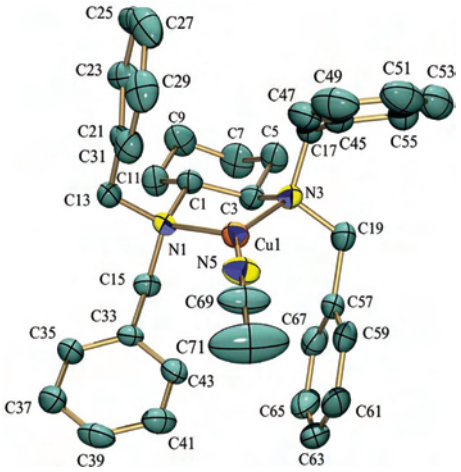

Figure 2. ORTEP representation (50% probability) of one monocation of the crystal structure of [**10a**·2CH_2Cl_2], excluding hydrogen atoms. Selected interatomic distances (Å) and angles (deg): Cu(1)−N(1), 2.094(3); Cu(1)−N(3), 2.082(3); Cu(1)−N(5), 1.870(4); N(5)−C(69), 1.114(5); N(1)Cu(1)N(3), 88.7(1); N(1)Cu(1)N(5), 132.3(1); N(3)Cu(1)-N(5), 139.0(1); Cu(1)N(5)C(69), 173.1(4).

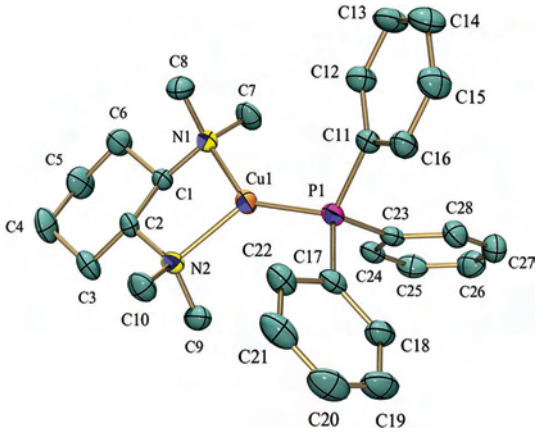

Figure 3. ORTEP representation (50% probability) of the monocation of **1d**, excluding hydrogen atoms. Selected interatomic distances (Å) and angles (deg): Cu(1)−N(1), 2.041(3); Cu(1)−N(2), 2.065(3); Cu(1)−P(1), 2.150(1); N(1)Cu(1)N(2), 88.2(1); N(1)Cu(1)P(1), 140.3(1); N(2)Cu(1)-P(1), 131.3(1).

defined in each case by the six carbon atoms of the nearest neighboring phenyl ring. Solutions of **10a** appeared to be air-stable upon standing for several days at 298 K; however, a CO adduct, [(**L**$^{\mathbf{TB}}$)Cu(CO)]CF_3SO_3, having an IR stretch of $\nu_{C\equiv O}$ = 2113 cm^{-1} formed readily upon exposure of a $CDCl_3$ solution of **10a** to $CO_{(g)}$ (1.7 atm, 15 min).

The auxiliary MeCN ligands in **1a**−**9a** are readily displaced by PPh_3; X-ray-quality crystals of a representative air-stable adduct, [(**L**$^{\mathbf{TM}}$)Cu(PPh_3)]CF_3SO_3, **1d**, were readily isolated following addition of a stoichiometric quantity of PPh_3 to an anaerobic CH_2Cl_2 solution of **1a**. The ^{1}H NMR spectrum of **1d** in the **L**$^{\mathbf{TM}}$ ligand region is analogous to that of **1a**, which was not isolated in solid form. The geometry about the Cu(I) center in **1d** is roughly trigonal-planar but is again distorted by the **L**$^{\mathbf{TM}}$ ligand bite angle of ∼88° (Figure 3); the Cu−N and Cu−P distances are unexceptional.

2:1 $_{rac}$L^{TM}/Cu(I) Complex. When a 2:1 $_{rac}$**L**$^{\mathbf{TM}}$/Cu stoichiometry is employed in place of an equimolar mixture, a colorless, air-stable compound, [($_{RR}$**L**$^{\mathbf{TM}}$)$_2$Cu]CF_3SO_3·

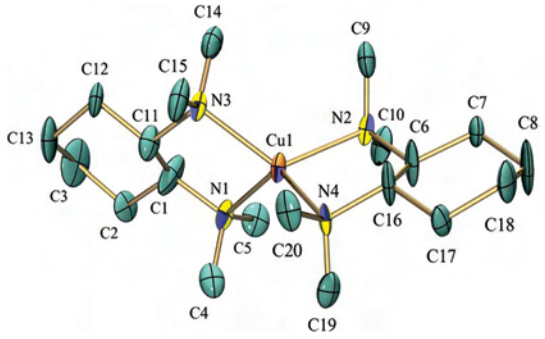

Figure 4. ORTEP representation (50% probability) of one monocation of **1c**, excluding hydrogen atoms. Selected interatomic distances (Å) and angles (deg): Cu(1)−N(1), 2.143(6); Cu(1)−N(2), 2.146(6); Cu(1)−N(3), 2.161(6); Cu(1)−N(4), 2.126(7); N(4)Cu(1)N(1), 122.5(3); N(4)Cu(1)-N(2), 84.8(3); N(1)Cu(1)N(2), 124.1(3); N(4)Cu(1)N(3), 122.8(3); N(1)-Cu(1)N(3), 84.7(3); N(2)Cu(1)N(3), 122.9(3). Note: atoms belonging to the depicted monocation are denoted in the tables[59] by the suffix 1.

[($_{SS}$**L**$^{\mathbf{TM}}$)$_2$Cu]CF_3SO_3 (**1c**), is isolated that presents an interesting case of ligand self-sorting (vide infra). Single crystals of the racemic[60] **1c** were characterized by X-ray diffraction (Figure 4, Table 2). Despite its tetragonal Laue symmetry, the crystal lattice in **1c** is best represented as two orthorhombic $P2_12_12_1$ unit cells twinned at a ∼45:55% ratio by interchange of the *a* and *b* axes. The asymmetric unit of each twin component contains two enantiomeric yet crystallographically unique monocations; if one of the pair is inverted, their coordinates are then isostructural to within 0.13 Å rms.[61] Relative to the 1:1 L/Cu(I) complexes reported above, the Cu−N_{amine} distances in **1c** (av 2.15(2) Å) are lengthened by 0.05−0.08 Å and the **L**$^{\mathbf{TM}}$ chelate bite angles are reduced by 3−4°, reflecting the electrostatic consequences of increased coordination number at a closed-shell d^{10} metal center.

Low-Temperature Oxygenation of 1a−9a and Characterization of Os. At appropriate concentrations,[62] the Cu(I) precursor complexes **1a**−**9a** react with dry O_2 at 193 K in CH_2Cl_2, THF, or acetone to afford the yellow- to red-brown, thermally unstable **O**s **1b**−**9b**, respectively. A 2:1 Cu/O_2 uptake stoichiometry was documented for several of these reactions by manometry (**3a**, **4a**, **5a**, **7a**; [Cu] = 30 mM, 1 atm O_2, CH_2Cl_2). The incorporated O_2 could not be reversibly displaced from any of the resulting **O**s by cycles of evacuation and purging with N_2, or by exposure to excess $CO_{(g)}$ (1 atm) or PPh_3 (∼100 equiv). EPR spectra at 77 K were essentially featureless for all **O**s; in no case did mononuclear Cu(II) signals account for more than 5% of

(60) A similar air-stable 2:1 L/Cu compound was also derived from enantiopure $_{RR}$**L**$^{\mathbf{TM}}$, but crystals suitable for diffraction could not be obtained.

(61) Considered separately, the monocations of **1c** obey the higher tetragonal space symmetry implied by the lattice dimensions: ignoring counterions, the model may be adequately represented in the space group *I*-42*d*, with each monocation residing on a crystallographic 2-fold axis and being related to the others by the principal 4-fold improper rotation axis.

(62) Oxygenation of **1a**, **2a**, or **6a** also gives rise to significant amounts of a 3:1 Cu/O_2 species when the Cu/O_2 concentration ratio is sufficiently greater than unity. We have previously reported structural[42] and spectroscopic[63,64] characterizations of the first of these, a trinuclear $[L_3Cu_3(\mu_3\text{-}O)_2]^{3+}$ complex; Itoh has also recently reported a similar 3:1 Cu/O_2 species.[30]

Table 3. Spectroscopic, Structural, and Thermal Decomposition Data for Selected **O**s[a]

ligand	**O**	$r_{Cu\cdots Cu}$ (Å) [r_{Cu-O} (Å)]	LMCT λ_{max} (nm) [ϵ (10^3 M^{-1} cm^{-1})]	rR shifts (cm^{-1}) $\nu^{16}O_2$ [$\nu^{18}O_2$] {$\Delta\nu$ ($^{16}O_2-^{18}O_2$)}	decay rate $T = 263$ K k_{obs} (s^{-1}) [$t_{1/2}$ (s)]	activation parameters $\Delta H^{\ddagger}$ (kJ mol^{-1}) [$\Delta S^{\ddagger}$ (J K^{-1} mol^{-1})]	ligand products % yield [theor max]
$\mathbf{L^{TM}}$	**1b**	−	301[b] [20] 399[b] [25]	605 [581][c] {23}	2.0×10^{-4} [3500]	56(1) [−102(5)]	30 [50][d]
$\mathbf{L^{EtMe_3}}$	**2b**	−	305 [19] 402 [27]	−	3.5×10^{-4} [2000]	−	−
$\mathbf{L^{ME}}$	**3b**	2.744,[e] 2.74[f,g] [1.802,[e] 1.81[f,g]]	313[b] [21] 408[b] [28]	610 [587][c] {23}	4.0×10^{-3} [170]	49(1) [−105(5)]	40 [50][h]
$\mathbf{L^{TE}}$	**4b**	−	319[b] [17] 413[b] [23]	616 [590][c] {26}	3.3×10^{-2} [21]	49(1)[i] [−84(4)][i]	50 [50]
$\mathbf{L^{TEED}}$	**5b**	2.74[f,g] [1.80][f,g]	307[b] [17] 407[b] [24]	603 [572][c] {31}	7.0×10^{-3} [100]	60(1)[i,j] [−54(4)][i,j]	30 [50]
$\mathbf{L^{(MeEt)_2ED}}$	**6b**	−	297 [23] 397 [25]	−	5.4×10^{-4} [1280]	−	8,[k] 5[l] [50]
$\mathbf{L^{Me_2Et_2ED}}$	**7b**	−	297 [18] 397 [21]	−	1.1×10^{-3} [630]	−	15 [50][h]
$\mathbf{L^{Me_3TACN}}$	**8b**	2.77[f,g] [1.81][f,g]	307[b] [16] 412[b] [18]	604 [581][c] {23}	1.7×10^{-2} [40]	52(1) [−78(4)]	22 [25][n]
$\mathbf{L^{Me_2ODACN}}$	**9b**	−	297 [16] 397 [15]	−	1.4×10^{-3} [500]	61(2) [−66(4)]	20 [25][n]
$\mathbf{L^{TMPD}}$ (Stack et al.)[m]	−	2.85[f] [1.81][f]	297[b] [16] 397[b] [24]	608 [581][c] {27}	−	−	−
$\mathbf{L^{Bn_3TACN}}$ (Tolman et al.)[o]	−	2.794[e] [1.81][e]	318 [12] 430 [14]	602/608[p] [583] {23}	9.6×10^{-2} [7]	58(2) [−41(5)]	40 [50]
$\mathbf{L^{Bu^t_2P(NSiMe_3)_2N}}$ (Hofmann et al.)[q]	−	2.906[e] [1.86][e]	315 [shoulder] 444 [10]	−	−	−	−
$\mathbf{L^{Me_2tmpa}}$ (Suzuki et al.)[s]	−	2.758[e] [1.80][e]	300 [12] 378 [19]	590 [564] {26}	−	−	−
$\mathbf{L^{Me_2etpy}}$ (Kitagawa, Suzuki et al.)[r]	−	2.866[e] [1.83][e]	— 390 [shoulder]	579 [551] {28}	−	−	−
$\mathbf{HMe_2L^{iPr_2}/L^{TMPD}}$ (Tolman et al.)[t]	−	2.849[e] [1.818][e]	— 398 [17]	653 [625] {28}	−	−	−
$\mathbf{L^{iPr_4dtne}}$ (Tolman et al.)[u]	−	2.783[e] [1.825][e]	316 [14] 414 [13]	600 [582] {18}	2.9×10^{-2} [24]	56(2) [−59(5)]	−

[a] All measurements were performed in CH_2Cl_2 solution except where otherwise noted. Listed concentrations and molar absorptivities are uncorrected for the thermal contraction of the solvent, which can be as great as 15%. [b] λ_{max} value includes a correction of +7 nm relative to previously reported values (refs 21, 66, and 69) to compensate for an instrument miscalibration. [c] See refs 21 and 66. [d] An additional formamide 4e$^-$ oxidation product ($\mathbf{L^{X+O}}$) is also observed for [Cu] = 2−5 mM (~5% [20% theor], [Cu] = 2.0 mM, 263 K). [e] Distance derived from crystal structure; Cu−O values are a molecular average. [f] Distance derived from solid-state EXAFS. [g] See refs 64 and 69. [h] $\mathbf{L^{X-Et}}$ only. [i] Equivalent kinetic results observed for THF and CH_2Cl_2 solutions. [j] Equivalent kinetic results observed for [**5b**·$(SbF_6)_2$] in THF. [k] $\mathbf{L^{X-Et}}$. [l] $\mathbf{L^{X-Me}}$. [m] $\mathbf{L^{TMPD}}$ = *N*,*N*,*N*′,*N*′-tetramethyl-1,3-propanediamine. See ref 22. [n] 4e$^-$ $\mathbf{L^{X+O}}$ formamide product only, [Cu] = 1.0 mM. [o] See refs 2 and 16. [p] Fermi doublet. [q] See ref 27. [r] See ref 49. [s] See ref 51. [t] Assembled in a stepwise process from [($\mathbf{HMe_2L^{iPr_2}}$)Cu(O_2)] and [($\mathbf{L^{TMPD}}$)Cu(MeCN)]$^+$; see ref 32. [u] See refs 2 and 17.

total Cu content. NMR susceptibility measurements[65] (190 K, CD_2Cl_2) did not indicate significant paramagnetism in any of the reported **O**s. The electronic absorption spectra of **1b**−**9b** exhibit characteristically intense ligand-to-metal charge transfer (LMCT) bands at $\lambda_{max} \approx 300$ (ϵ = 10 000−20 000 M^{-1} cm^{-1}) and 400 nm (ϵ = 10 000−30 000 M^{-1} cm^{-1}). The LMCT-enhanced ($\lambda_{excitation}$ = 407 nm) resonance Raman (rR) spectra of **1b**, **3b**, **4b**, **5b**, and **8b** contain similarly intense O_2 isotope-sensitive peaks at ~600 cm^{-1}. These spectroscopic features and rR O_2-isotope shifts[21,66] are summarized in Table 3 together with those of other pertinent literature examples.

Crystal Structure of [($\mathbf{L^{ME}}$)$_2$Cu$_2$(μ−O)$_2$](CF$_3$SO$_3$)$_2$·4CH$_2$Cl$_2$. Thermally sensitive crystals of [**3b**·$4CH_2Cl_2$] were grown from a concentrated CH_2Cl_2 solution by layering with Et_2O at 193 K. These were characterized by X-ray diffraction (Table 2); relevant metrical parameters are summarized in Figure 5. The well-ordered asymmetric unit contains a crystallographically unique binuclear [($\mathbf{L^{ME}}$)$_2$Cu$_2$(μ-O)$_2$] cluster in which the dioxygen O−O bond has been cleaved (O···O, 2.334 Å). The most striking metrical features are the extremely short Cu−O bonds at both Cu centers (av Cu−O, 1.802(7) Å) and the short Cu···Cu separation (2.744(1) Å). The two noncoordinating $CF_3SO_3^-$ ions present in the asymmetric unit imply a net 2+ charge on the cation. Each Cu atom is ligated in an approximately square-planar [N_2O_2]

(63) Root, D. E.; Henson, M. J.; Machonkin, T.; Mukherjee, P.; Stack, T. D. P.; Solomon, E. I. *J. Am. Chem. Soc.* **1998**, *120*, 4982−4990.
(64) Dubois, J. L.; Mukherjee, P.; Stack, T. D. P.; Hedman, B.; Solomon, E. I.; Hodgson, K. O. *J. Am. Chem. Soc.* **2000**, *122*, 5775−5787.
(65) Evans, D. F. *J. Chem. Soc.* **1959**, 2003−2005.
(66) Henson, M. J.; Mukherjee, P.; Root, D. E.; Stack, T. D. P.; Solomon, E. I. *J. Am. Chem. Soc.* **1999**, *121*, 10332−10345.

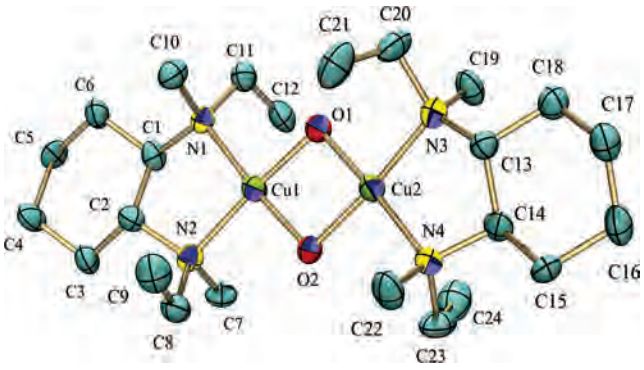

Figure 5. ORTEP representation (50% probability) of the dication of [**3b**·4CH_2Cl_2], excluding hydrogen atoms. Selected interatomic distances (Å) and angles (deg): Cu(1)−O(1), 1.809(6); Cu(1)−O(2), 1.808(6); Cu(2)−O(1), 1.795(5); Cu(2)−O(2), 1.799(6); Cu(1)···Cu(2), 2.744(1); O(1)···O(2), 2.334(1); O(2)Cu(1)O(1), 80.4(2); N(1)Cu(1)N(2), 89.9(3); O(1)Cu(2)O(2), 81.0(2); N(4)Cu(2)N(3), 89.3(3); Cu(2)O(1)Cu(1), 99.2(3); Cu(2)O(2)Cu(1), 99.1(3).

environment; however, the [$Cu_2O_2N_4$] core as a whole is slightly twisted, with a dihedral angle of 7.5(2)° between the two [N_2CuO_2] planes. A highly ordered, pseudo-C_2-symmetric alternation of *N*-ethyl and *N*-methyl substituents within and between the ligands is observed. This arrangement places one methylene proton on each of the four *N*-ethyl substituents in proximity to the bridging oxide ligands (C8−H8A···O2, 2.51 Å; C11−H11A···O1, 2.47 Å; C20−H20B···O1, 2.60 Å; C23−H23B···O2, 2.60 Å). Restrained refinement of the *N*-methyl hydrogens converges to the expected staggered conformation in each case, thus placing the four proximate methyl protons at somewhat greater average distance from the oxide ligands (C7−H7A···O2, 2.69 Å; C10−H10B···O1, 2.63 Å; C19−H19B···O1, 2.72 Å; C22−H22B···O2, 2.58 Å).

Formation Kinetics. In general, the diffusion-limited formation of **1b**−**9b** from **1a**−**9a** proceeds rapidly in O_2-saturated CH_2Cl_2, acetone, or THF, with full **O** formation occurring in ∼10−15 s (1 atm O_2, [Cu] = 0.1−2.0 mM, 193 K).[67] The sole exception to this norm, apart from the wholly inert **10a** (q.v.), is **4a**, the oxygenation of which proceeds with like alacrity in pure acetone or THF but requires ∼2 h for completion in pure, O_2-saturated CH_2Cl_2. A pseudo-first-order rate constant of $k_{obs} = 4.4 \times 10^{-4}$ s^{-1} was obtained for the latter case by means of a multivariate spectral analysis in which absorbance data (λ = 280−450 nm) were fitted to a simple first-order A → B model. No colored intermediate species were noted. The reaction was also followed in O_2-saturated 1:1 (v/v) THF/CH_2Cl_2 by monitoring the optical absorbance of a characteristic LMCT band due to **4b** (λ_{max} = 413 nm) during the initial 5% (200 s) of the reaction coordinate (0.2 < [**4a**]$_0$ < 2.0 mM, 1 atm O_2, 193 K). A plot of log rate$_{initial}$ vs log [**4a**]$_0$ showed a linear relationship corresponding to a rate law that is first-order in [**4a**] with $k_{obs} = 2.5 \times 10^{-3}$ s^{-1} under the above conditions;[59] multivariate analyses (280−450 nm) of multiple spectroscopic runs gave $k_{obs} = 2.3 \times 10^{-3}$ s^{-1} for this mixed-solvent system. An Eyring fit comprising k_{obs} values measured between 195 and 213 K yielded activation parameters $\Delta H^{\ddagger}$ = 25(4) kJ mol^{-1}/6(1) kcal mol^{-1} and $\Delta S^{\ddagger}$ = −210(40) J K^{-1} mol^{-1}/−50(10) cal K^{-1} mol^{-1}; the accessible temperature range for kinetic experiments was constrained by the freezing point of the solvent and the onset of rapid thermal decomposition of **4b** above 213 K.

Reactivity with Exogenous Substrates. O complexes **1b**−**7b** were screened against several organic substrates in order to determine the characteristic reactivity of the **O** core. Typically, solutions of each **O** ([Cu] = 1.0 mM) were treated with 1−5 equiv of substrate at 193 K under a N_2 atmosphere, and the ensuing reactions were allowed to proceed until either the characteristic UV−vis absorption features of the **O** chromophore had been quenched or the maximum interval of 6 h had elapsed. After workup, the organic products were assayed by GC-MS and/or ^{1}H NMR spectroscopy (generally, the Cu products were not characterized). **O**s **1b**−**7b** reacted rapidly in >95% yield with 2 equiv of 2,4-di-*tert*-butylphenol (DBP), thiocresol, or *tert*-butylthiol to give 3,3′,5,5′-tetra-*tert*-butyl-2,2′-bis(phenol), 4-methylphenyl disulfide, or *tert*-butyl disulfide, respectively, but showed no apparent reactivity (<5% yield) toward ethylene, cyclohexene, 1,4-cyclohexadiene, 9,10-dihydroanthracene, xanthene, fluorene, $(CH_3)_2S$, $(CH_3)_2SO$, or $PhSCH_3$ (1−5 equiv). These results are summarized in Scheme 2. Reaction of **1b**−**7b** with the lithium alkoxide salts of benzyl and cinnamyl alcohols (2 equiv) rapidly gave the corresponding aldehydes in >95% yield, whereas the alcohols themselves displayed minimal (<5%) reactivity even upon warming (233 K). A representative aliphatic primary alcohol, 1-octanol (2 equiv), was similarly unreactive even when deprotonated. Spectrophotometric titrations of **1b**−**5b** (193 K, N_2) with 2 equiv of ferrocene (Fc) or decamethylferrocene ($Me_{10}Fc$) quenched the characteristic LMCT optical bands, whereas 1.5 equiv of acetylferrocene (AcFc) was unreactive through 6 h in all cases.

Bis(μ-hydroxo)dicopper(II) Dimers. The bis(μ-hydroxo)-dicopper(II) dimer [(**L**^{TM})$_2$$Cu_2$(μ-OH)$_2$]($CF_3SO_3$)$_2$ ($_{RR,RR}$**1e**) was synthesized in near-quantitative yield via reaction of **1b** with 2 equiv of a sacrificial 1e$^-$, 1H$^+$ donor such as DBP or *tert*-butylthiol and was also isolated in lesser yield (60%) from thermally decomposed solutions of **1b**. The racemic dimer [($_{SS}$**L**^{TM})($_{RR}$**L**^{TM})Cu_2(μ-OH)$_2$](CF_3SO_3)$_2$ ($_{RR,SS}$**1e**) was obtained in an analogous manner using $_{rac}$**L**^{TM}. In contrast to **1b**, $_{RR,RR}$**1e** and $_{RR,SS}$**1e** are stable indefinitely at 293 K in aprotic solvents, and their electronic spectrum (λ_{max} = 269 nm; ϵ = 14 000 M^{-1} cm^{-1}) contain no low-energy (>300 nm) LMCT bands.

Both $_{RR,RR}$**1e** and $_{RR,SS}$**1e** were structurally characterized (Table 2). The enantiomerically pure $_{RR,RR}$**1e** crystallizes in the acentric group $P2_1$ (Figure 6). Both Cu(II) atoms are coordinated in an approximately square-planar geometry, with no unusual bond distances and a substantially larger Cu···Cu separation (2.99 Å) relative to all structurally characterized **O**s (Table 3). Each bridging hydroxo ligand participates in a hydrogen-bonding interaction with a triflate

(67) The manner in which O_2 is introduced into the reaction vessel has a significant effect on formation rates. For example, full formation of **1b** at 193 K is complete within 10 s if concentrated **1a** is injected into O_2-saturated CH_2Cl_2 but requires several minutes if O_2 is introduced afterwards by bubbling.

Scheme 2. Reactivity of Selected **O**s toward Exogenous Substrates[a]

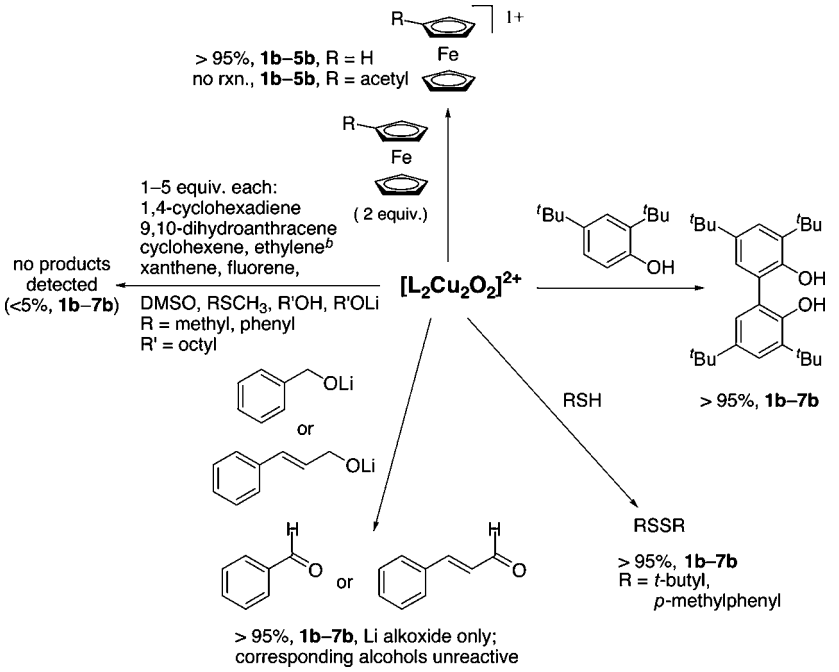

[a] Conditions (unless otherwise stated): 193 K, CH_2Cl_2, N_2 atmosphere, 2 equiv of substrate/**O**, max 6 h. [b] 1 atm.

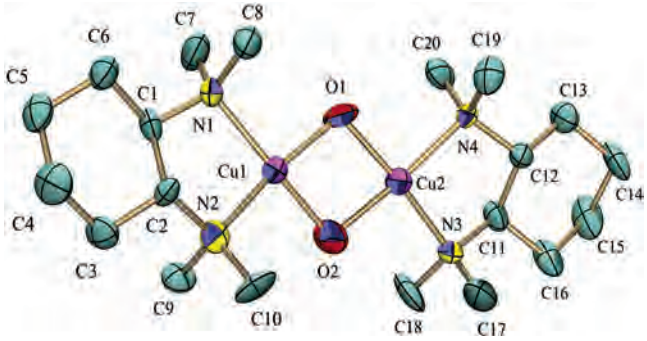

Figure 6. ORTEP representation (50% probability) of the dication of *RR,RR*-**1e**, excluding hydrogen atoms. Selected interatomic distances (Å) and angles (deg): Cu(1)−O(1), 1.89(1); Cu(1)−O(2), 1.917(8); Cu(2)−O(1), 1.916(8); Cu(2)−O(2), 1.92(1); Cu(1)···Cu(2), 2.990(2); O(1)···O(2), 2.37; O(1)Cu(1)O(2), 77.1(4); N(2)Cu(1)N(1), 86.7(4); O(1)Cu(2)O(2), 76.5(4); N(3)Cu(2)N(4), 87.4(4); Cu(1)O(1)Cu(2), 103.5(5); Cu(1)O(2)Cu(2), 102.5(5).

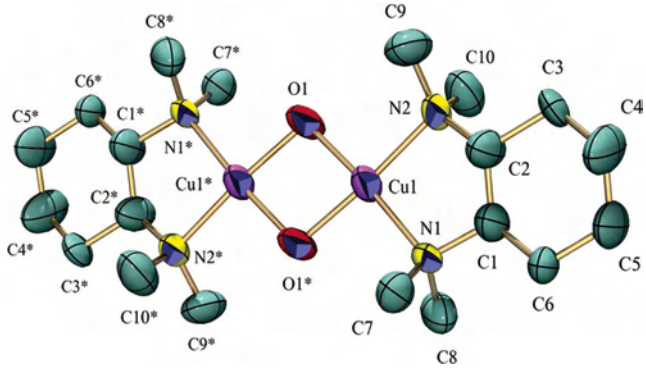

Figure 7. ORTEP representation (50% probability) of the dication of *RR,SS*-**1e**, excluding hydrogen atoms. Asterisks denote inversion-related atoms. Selected interatomic distances (Å) and angles (deg): Cu(1)−O(1), 1.913(8); Cu(1)−O(1*), 1.908(8); Cu(1)···Cu(1*), 2.985(3); O(1)···O(1*), 2.39; O(1*)Cu(1)O(1), 77.3(4); N(1)Cu(1)N(2), 87.1(4); Cu(1*)O(1)-Cu(1), 102.7(4).

oxygen atom (O1···O7, 2.89(2) Å; O2···O5, 2.94(2) Å). Although each half of the *RR,RR*-**1e** dimer is crystallographically unique, the two parts are superimposable and isostructural to within 0.1 Å rms. The least-squares planes defined by each respective $[N_2CuO_2]$ unit are twisted by 12.5° relative to one another, a distortion mandated by the chirality of the ligand.

By contrast, the racemic *RR,SS*-**1e** crystallizes in a centrosymmetric space group and contains one ligand of *RR* type and one of *SS* type, with each heterochiral cation resting on a crystallographic inversion center (Figure 7). Thus, neither intra- nor intermolecular spontaneous resolution to homochiral enantiomers is observed in the solid state, and the Cu, N, and O atoms of *RR,SS*-**1e** are rigorously coplanar as required by crystallographic symmetry. Bond distances are again typical of Cu(II) complexes, and weak hydroxo−triflate hydrogen-bonding interactions similar to those of *RR,RR*-**1e** are also evident (O1···O7, 3.09(2) Å).

Thermal Decomposition. The thermal decomposition kinetics of **1b**−**9b** were studied by UV−vis spectroscopy and multivariate spectral analysis. The time-dependent evolution of the absorbance profile (λ = 280−450 nm) was successfully fitted in each case to a simple first-order A → B model involving two principal colored components. Decomposition rate constants (k_{obs}) obtained in this manner for complexes **1b**, **3b**, **4b**, **5b**, **8b**, and **9b** at temperatures between 223 and 293 K[68] were used to generate Eyring plots[59] from which the activation parameters $\Delta H^{\ddagger}$ and $\Delta S^{\ddagger}$ were derived (Table 3). Primary kinetic isotope effect (KIE) values for the thermal decay of **1b** and **3b** were obtained through experiments conducted with the corresponding

(68) **1b**: 293−263 K, [Cu] = 1.0 mM, CH_2Cl_2; **3b**: 280−248 K, [Cu] = 1.0 mM, CH_2Cl_2; d_8-**3b**: 291−253 K, [Cu] = 1.0 mM, CH_2Cl_2; **4b**: 263−223 K, [Cu] = 1.0 mM, THF; **5b**: 263−233 K, [Cu] = 1.0 mM, THF; **8b**: 263−233 K, [Cu] = 0.2 mM, CH_2Cl_2; **9b**: 278−243 K, [Cu] = 1.0 mM, CH_2Cl_2.

deuterated ligands d_{12}-$\mathbf{L^{TM}}$ (perdeuterated methyl groups) and d_4-$\mathbf{L^{ME}}$ (deuterated *N*-methylene only). For **1b**/d_{24}-**1b**, a primary KIE value of $k_{obs}^{H}/k_{obs}^{D} \approx 8$ was observed at 293 K, whereas for **3b**/d_8-**3b**, a primary KIE value of $k_{obs}^{H}/k_{obs}^{D} \approx 3$ was calculated for $T = 293$ K by extrapolation from linear Eyring equation fits. For each decomposed **O**, the corresponding ligand products were recovered and analyzed. Reproducible ratios of unchanged ligand ($\mathbf{L^X}$) to monodealkylated products indicative of $2e^-$ oxidation ($\mathbf{L^{X-R}}$) and/or oxygenated formamide products indicative of $4e^-$ oxidation ($\mathbf{L^{X+O}}$) were quantified by GC-MS (Table 3); the latter were observed as minor products at higher concentrations of **1b** ([Cu] = 2−5 mM) and were the major ligand products recovered from the thermal decay of **8b** and **9b**.

Discussion

Ramifications of Ligand Design. A recently published analysis[70] of theoretical calculations[46,71,72] that address the relative energies of isomeric μ-η^2:η^2-peroxodicopper(II) (**P**) and bis(μ-oxo)dicopper(III) (**O**) complexes underscores the central role of ligand structure in determining the nature and distribution of $Cu-O_2$ species within a given coordination environment. Ligand steric demands, denticity, chelation geometry, and donor characteristics are critical factors. For example, simple bidentate 1,2-PDLs differentiated solely on the basis of *N*-alkyl substituent size and conformational rigidity support a range of species encompassing 2:1 (**P**[34,35] and **O**[21,22]), 3:1 (trinuclear),[42] and 4:1[40,73] Cu/O_2 reaction stoichiometries; a similar trend was also recently reported for a series of 2-(2-pyridyl)ethylamines.[30] Likewise, backbone perturbations within a family of β-diketiminate ligands are reported to facilitate selective formation of charge-neutral [$LCu(O_2)$] (1:1) and **O** (2:1) species.[31−33,74] Studies of interconverting **P**/**O** systems demonstrate that the distribution of species may be manipulated through the use of appropriate solvents and counteranions.[35,44,75,76] The variation of secondary electronic characteristics within a ligand family has also demonstrated usefulness in fine-tuning such equilibria.[77]

Although frequently observed in natural Cu proteins, axial ligation is not a requisite condition for supporting $Cu-O_2$ intermediates. Electrochemical studies[78−81] and theoretical calculations[70,82] indicate that the Cu(III) d^8 system prefers a rigorously square-planar coordination environment given a ligand field of sufficient strength, which suggests that bidentate strong σ-donor ligands with constrained bite angles near 90° should provide optimal thermodynamic stabilization of the d^8 Cu(III) sites in the **O** core. Comparison of **O**s based on tridentate and bidentate amine ligands reveals extensive spectroscopic and structural similarity (Table 3). Yet tridentate amine ligands give rise to 5-coordinate [N_3O_2] Cu(III) sites with weakly bound axial nitrogen donors that restrict physical access to the $[Cu_2O_2]^{2+}$ core relative to a more open [N_2O_2] square-planar coordination environment. Such accessibility is essential to inner-sphere oxidative processes that involve exogenous substrates.[22] Its importance is well documented in the case of Hc, which can acquire phenol oxidase activity via removal of residues that block direct substrate access.[83,84] A similar concept may also underlie the catalytic activity of tyrosinase: in its oxygenated form, the tertiary structure of this Cu monooxygenase allows substrates freer access to the **P** core than does its nonenzymatic, spectroscopically analogous counterpart oxyHc.[85,86]

Chirality and Conformational Rigidity. Both ED and CD provide convenient, modular synthetic access to a homologous series of simple Cu(I)-complexing PDLs (Scheme 1) that possess the essential ligating characteristics necessary to support generation of **O**s. These ligands span a steric continuum within which the nature of the proximal *N*-alkyl substituents may be incrementally varied, allowing systematic study of the effects of ligand design on the formation, stability, and reactivity of these complexes. In this context, the CD backbone affords several refinements relative to ED. In the most thermodynamically stable "chair" conformation, the two trans amino groups are equatorially oriented, creating a highly predisposed binding pocket for coordination of transition metals. CD is also optically active, and its enantiomers are conveniently resolved.[87] The use of a conformationally restricted enantiopure ligand in the spontaneous self-assembly of dimers significantly reduces the likelihood of obtaining multiple diastereomeric products or conformers of products,[88−90] and it offers the additional

(69) Dubois, J. L.; Mukherjee, P.; Collier, A. M.; Mayer, J. M.; Solomon, E. I.; Hedman, B.; Stack, T. D. P.; Hodgson, K. O. *J. Am. Chem. Soc.* **1997**, *119*, 8578−8579.
(70) Siegbahn, P. E. M. *J. Biol. Inorg. Chem.* **2003**, *8*, 577−585.
(71) Bérces, A. *Inorg. Chem.* **1997**, *36*, 4831−4837.
(72) Flock, M.; Pierloot, K. *J. Phys. Chem. A* **1999**, *103*, 95−102.
(73) Mukherjee, P. Ph.D. Thesis, Stanford University, 2000.
(74) Aboelella, N. W.; Kryatov, S. V.; Gherman, B. F.; Brennessel, W. W.; Young, V. G.; Sarangi, R.; Rybak-Akimova, E. V.; Hodgson, K. O.; Hedman, B.; Solomon, E. I.; Cramer, C. J.; Tolman, W. B. *J. Am. Chem. Soc.* **2004**, *126*, 16896−16911.
(75) Cahoy, J.; Holland, P. L.; Tolman, W. B. *Inorg. Chem.* **1999**, *38*, 2161−2168.
(76) Liang, H. C.; Henson, M. J.; Hatcher, L. Q.; Vance, M. A.; Zhang, C. X.; Lahti, D.; Kaderli, S.; Sommer, R. D.; Rheingold, A. L.; Zuberbuhler, A. D.; Solomon, E. I.; Karlin, K. D. *Inorg. Chem.* **2004**, *43*, 4115−4117.
(77) Henson, M. J.; Vance, M. A.; Zhang, C. X.; Liang, H. C.; Karlin, K. D.; Solomon, E. I. *J. Am. Chem. Soc.* **2003**, *125*, 5186−5192.
(78) Bossu, F. P.; Chellappa, K. L.; Margerum, D. W. *J. Am. Chem. Soc.* **1977**, *99*, 2195−2203.
(79) Youngblood, M. P.; Margerum, D. W. *Inorg. Chem.* **1980**, *19*, 3068−3072.
(80) Ruiz, R.; Surville-Barland, C.; Aukauloo, A.; Anxolabehere-Mallart, E.; Journaux, Y.; Cano, J.; Muñoz, M. C. *J. Chem. Soc., Dalton Trans.* **1997**, 745−751.
(81) Cervera, B.; Sanz, J. L.; Ibáñez, M. J.; Vila, G.; Lloret, F.; Julve, M.; Ruiz, R.; Ottenwaelder, X.; Aukauloo, A.; Poussereau, S.; Journaux, Y.; Muñoz, M. C. *J. Chem. Soc., Dalton Trans.* **1998**, 781−790.
(82) Liu, X. Y.; Palacios, A. A.; Novoa, J. J.; Alvarez, S. *Inorg. Chem.* **1998**, *37*, 1202−1212.
(83) Decker, H.; Dillinger, R.; Tuczek, F. *Angew. Chem., Int. Ed.* **2000**, *39*, 1591−1595.
(84) Decker, H.; Tuczek, F. *Trends Biochem. Sci.* **2000**, *25*, 392−397.
(85) Jaenicke, E.; Decker, H. *ChemBioChem* **2004**, *5*, 163−169.
(86) Decker, H.; Jaenicke, E. *Dev. Comp. Immunol.* **2004**, *28*, 673−687.
(87) Whitney, T. A. *J. Org. Chem.* **1980**, *45*, 4214−4216.
(88) Enemark, E. J.; Stack, T. D. P. *Angew. Chem., Int. Ed. Engl.* **1995**, *34*, 996−998.
(89) Enemark, E. J.; Stack, T. D. P. *Angew. Chem., Int. Ed.* **1998**, *37*, 932−935.
(90) Masood, M. A.; Enemark, E. J.; Stack, T. D. P. *Angew. Chem., Int. Ed.* **1998**, *37*, 928−932.

prospect of asymmetric induction in reactions with exogenous substrates.[91]

As is customary, peripheral ligand alkyl groups are employed to preclude the formation of a 2:1 L/Cu square-planar Cu(II) complex via spontaneous disproportionation of the Cu(I) precursor. With a sterically compact ligand such as $\mathbf{L^{TM}}$, formation of a 2:1 $[L_2Cu]^{1+}$ Cu(I) complex is also possible (**1c**, Figure 4), but the proximity of the ligand *N*-alkyl substituents enforces a tetrahedral coordination geometry that stabilizes the Cu(I) oxidation state. Accordingly, **1c** is inert to O_2 in the solid state even at 298 K. Its crystal structure provides an elegant example of intramolecular chiral self-recognition, such as we have previously reported[90] for Cu(I) complexes of other $_{rac}$CD-based ligands: although synthesized from $_{rac}\mathbf{L^{TM}}$, **1c** is composed exclusively of homochiral units in the solid state.[60] Comparison of the energies derived from hybrid DFT calculations on homochiral (**1c**) and heterochiral ($_{RR,SS}$**1c**) formulations suggests that the homochiral complex is more thermodynamically stable than its hypothetical centrosymmetric counterpart by $\Delta\Delta G^\circ \approx 0.9$ kcal mol^{-1} at 298 K.[59] The influence of ligand chirality on the structures of self-assembled complexes is further illustrated by comparison of the crystal structures of the bis(μ-hydroxo)dicopper(II) dimers $_{RR,RR}$**1e** and $_{RR,SS}$**1e**: the homochiral $\mathbf{L^{TM}}$ ligands of the former impart a 12.5° twisting distortion to its $[N_4Cu_2O_2]$ basal plane, whereas the inversion-related ligand pair in $_{RR,SS}$**1e** gives rise to a planar $[N_4Cu_2O_2]$ unit.

O_2 Reactivity of 1:1 L/Cu(I) Complexes. The reaction of each ligand with $[Cu(MeCN)_4]CF_3SO_3$ at 1:1 stoichiometry yields a discrete, monocationic Cu(I) complex with at least one MeCN molecule bonded as a labile auxiliary. The ^{1}H NMR symmetry and chemical shifts of these complexes are consistent with either a tetrahedral 4-coordinate $[LCu(MeCN)_2]^{1+}$ formulation or a trigonal-planar 3-coordinate $[LCu(MeCN)]^{1+}$ configuration like that observed in the solid-state structures of **4a** and **10a**. If the former species is present, the rapid exchange of MeCN observed by NMR implies a facile equilibrium with the latter. Given the presumed associative nature of O_2 binding (vide infra), we believe that such 3-coordinate $[LCu(MeCN)]^{1+}$ species are the active precursors in the formation of Cu−O_2 species with bidentate ligands. A recent study of host−guest exchange interactions between tridentate calix[6]arene−Cu(I) complexes and auxiliary nitrile proligands indicates that the large enthalpic cost of Cu(I)−nitrile bond scission is significantly offset by the favorable entropic contribution arising from the overall increase in the number of particles upon dissociation of the nitrile from the complex.[92] The structurally characterized Cu(I) species $[\{(-)\text{-sparteine}\}Cu(MeCN)_2]CF_3SO_3$, which is 4-coordinate in the solid state, reacts readily with O_2 at low temperatures to form an **O**;[25] again, a facile equilibrium between 3- and 4-coordinate species is presumed to be essential to the observed O_2 reactivity.

Crystal Structure of [3b·4CH_2Cl_2]. Low-temperature crystallography of Cu−O_2 species is frequently hampered by substantial disorder and other intrinsic problems that lead to high residual values when refining against all intensity data. In this context, the solid-state structure of [**3b**·$4CH_2Cl_2$] (Figure 5) is notable for its high data redundancy (~12 observations per refined parameter), low residual values ($R_1 = 5.5\%$; $wR_2 = 12.9\%$ on F^2), the absence of significant solvent or counteranion disorder, and the fact that its species of interest occupies a general position (as opposed to a special position, or symmetry element). The metrical parameters of the **O** core in the crystal structure closely correspond to those derived from solid-state EXAFS (vide infra).[64,69] The refined model provides insight into the constraints imposed by the chiral $\mathbf{L^{ME}}$ ligands on the self-assembly of **3b**. The alternating "up, down" geared intra- and interligand arrangement of the *N*-ethyl and *N*-methyl substituents (Figure 5) affords steric protection to the **O** core while minimizing energetically unfavorable interligand interactions: the closest approach of any pair of terminal substituent carbon atoms on alternate ligands is 4.57 Å (C10···C21). The homochirality of the $_{RR}\mathbf{L^{ME}}$ ligands imparts a slight ~8° twist to the basal $[N_2CuO_2CuN_2]$ unit, similar to that observed in the homochiral bis(μ-hydroxo)dicopper(II) dimer $_{RR,RR}$**1e** (vide supra). The observed intramolecular C−H···O interactions between the alkyl substituent NC^α protons and the bridging oxide ligands have been noted in reports of other structurally characterized **O**s[16,51] and are suggestive of the proposed thermal decomposition mechanism, which involves selective C−H bond cleavage at these positions (vide infra).

Among structurally characterized **O**s, **3b** is the most metrically compact example yet documented. It belongs to a group of several among which the Cu···Cu distance varies by only 0.05 Å (L = $\mathbf{L^{ME}}$, av Cu−O 1.802(7) Å, Cu···Cu 2.744(1) Å; $\mathbf{L^{Bn_3TACN}}$, av Cu−O 1.81 Å, Cu···Cu 2.794 Å;[16] $\mathbf{L^{iPr_4dtne}}$, av Cu−O 1.825 Å, Cu···Cu 2.783 Å;[17] $\mathbf{L^{Me_2tmpa}}$, av Cu−O 1.80 Å, Cu···Cu 2.76 Å;[49] Table 3). For L = $\mathbf{L^{Bn_3TACN}}$, e.g., the $[Cu_2O_2]$ fragment is isostructural with that of [**3b**·$4CH_2Cl_2$] to within 0.046 Å rms, and the $[Cu_2N_4O_2]$ fragment to within 0.094 Å rms. All of these **O**s are based on ligands that form five-membered chelate rings with the Cu ions. **O** complexes that contain six-membered chelate rings, by contrast, exhibit longer Cu···Cu separations (2.866 Å, L = $\mathbf{L^{Me_2etpy}}$;[51] 2.849 Å, $[(\mathbf{HMe_2L^{iPr_2}})Cu(\mu\text{-}O)_2Cu(\mathbf{L^{TMPD}})]CF_3SO_3$;[32] 2.85 Å (EXAFS), L = $\mathbf{L^{TMPD}}$ = *N*,*N*′,*N*′-tetramethyl-1,3-propanediamine). This elongation of the Cu···Cu distance reflects a greater degree of steric interaction within the **O** core, likely due to the larger bite angle of such ligands. The thermally stable **O** reported by Hofmann and colleagues[27] also exhibits significantly divergent metrical features relative to **3b** (Cu−O 1.86 Å, Cu···Cu 2.906 Å). This charge-neutral complex is based on an anionic, strongly basic iminophosphanamide ligand that forms a four-membered chelate and thus represents a quite different geometric and electronic coordination profile.

The observed thermal lability, short Cu···Cu and Cu−O distances, and absence of close contacts between the bridging

(91) Yoon, T. P.; Jacobsen, E. N. *Science* **2003**, *299*, 1691−1693.
(92) Rondelez, Y.; Rager, M.-N.; Duprat, A.; Reinaud, O. *J. Am. Chem. Soc.* **2002**, *124*, 1334−1340.

oxides and the counteranions clearly differentiate [**3b**·$4CH_2Cl_2$] from the superficially similar bis(μ-hydroxo)dicopper(II) complexes $_{RR,RR}$**1e** and $_{RR,SS}$**1e**. Yet the +3 oxidation state of the Cu centers in **3b** and other **O**s cannot be deduced from their crystal structures alone, since no substantially disparate Cu−O bond distances are present to allow for an internal comparison[42,64] and since similarly short Cu−O bonds are observed, albeit rarely, among authentic Cu(II) compounds.[15,93,94] Moreover, in complexes that exhibit substantial metal−ligand covalency, formally assigned oxidation states are of dubious significance unless based upon a direct probe of the electron density at the metal center.[64,95] In the case of **3b**, a comparative Cu K-edge XAS study using the structurally related $_{RR,RR}$**1e** as a reference unambiguously indicated a formal +3 oxidation state for both Cu atoms.[64,69] The spectroscopically analogous species **1b**−**9b**, accordingly, are all best described as bis(μ-oxo)dicopper(III) complexes. The XAS technique remains the sole experimental basis for definitive assignment of valence in this class of compounds.

Spectroscopy. Together with the observed diamagnetism, the intense LMCT and O_2 isotope-sensitive rR features exhibited by **1b**−**9b** are diagnostic for **O**s,[66] as the characteristic maxima for other 2:1 Cu−O_2 chromophores appear at different energies (**P**: LMCT ∼360 and ∼540 nm, rR ν_{O-O} ∼720−760 cm^{-1}; *trans*-μ-1,2-peroxo: LMCT ∼520−550 and ∼600−630 nm, rR ν_{O-O} ∼830 cm^{-1} and ν_{Cu-O} ∼550 cm^{-1}).[1,96] The intensity of the LMCT absorptions (ϵ = 10 000−30 000 M^{-1} cm^{-1}) indicates substantial covalency in the Cu(III)−O^{2-} interaction. On the basis of electronic structure calculations and rR studies, the ∼300 nm band has been assigned to the oxygen in-plane $\pi_\sigma^* \rightarrow$ Cu(III) d_{xy} LMCT and the ∼400 nm band to the oxygen $\sigma_u^* \rightarrow$ Cu(III) d_{xy} LMCT.[97]

The rR spectra of several **O**s reported herein were the subject of recent detailed theoretical and experimental studies in which most of the prominent features were assigned (Table 3).[26,66] These include characteristically intense fundamental bands at ∼120 and ∼600 cm^{-1} that are enhanced upon excitation into the ∼400 nm LMCT transition. The isotopic shift of the ∼600 cm^{-1} feature on substitution of $^{16}O_2$ with $^{18}O_2$ ($\Delta\nu(^{16}O_2-^{18}O_2) \approx 26$ cm^{-1}) is consistent with its assignment as an A_g-symmetric [Cu_2O_2] synchronous "breathing" mode involving substantial elongation along the Cu−O bond vectors (Scheme 3). The O_2 isotope insensitivity of the ∼120 cm^{-1} feature comports with its assignment as a symmetrical, pairwise antisynchronous "flexing" mode, which primarily involves changes in the internal angles of the [Cu_2O_2] rhomb (Scheme 3).[66] Analogous rR features have been observed for other metal bis(μ-oxo) M_2O_2 cores (M = Ni, Co, Fe, and Mn).[26]

The homologous series of enantiopure CD ligands employed in this work (Table 1) provides an excellent platform for examining spectroscopic trends because the corresponding **O**s contain exclusively homochiral ligands locked into a single backbone conformation. Systematic increases in *N*-alkyl substituent steric demands within the series produce subtle but significant corresponding bathochromic shifts in both the higher- and lower-energy LMCT bands of the **O** chromophore (**1b**: 301, 399 nm; **2b**: 305, 402 nm; **3b**: 313, 408 nm; **4b**: 319, 413 nm). We attribute this general phenomenon primarily to sterically induced perturbations of the **O** core geometry: as peripheral ligand bulk increases, the [Cu_2O_2] rhomb elongates, increasing the Cu···Cu separation while decreasing the O···O separation. Since the donor orbitals for both LMCT transitions are antibonding with respect to a potential O−O interaction, a shortening of the O···O distance should raise their energies relative to that of the Cu(III) d_{xy} acceptor MO. This trend is borne out among [9]ane-based **O**s (**8b**: Cu···Cu 2.77 Å, LMCT 307 and 412 nm; [($\mathbf{L}^{\mathbf{iPr_4dtne}}$)$Cu_2(\mu\text{-}O)_2$]$^{2+}$: Cu···Cu 2.78 Å, LMCT 316 and 414 nm;[17] [($\mathbf{L}^{\mathbf{Bn_3TACN}}$)$_2Cu_2(\mu\text{-}O)_2$]$^{2+}$: Cu···Cu 2.79 Å, LMCT 318 and 430 nm[16]).

Scheme 3. Resonance Raman-Active A_g-Symmetric Principal Vibrational Modes of **O** Complexes[66]

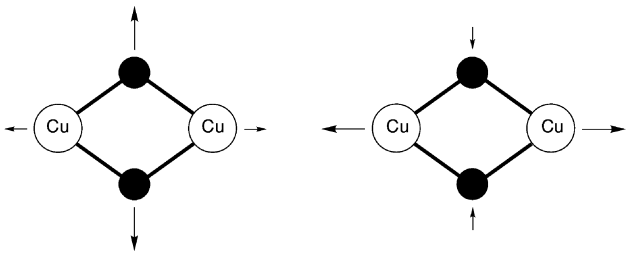

Twisting of the ligand N−Cu−N chelate planes relative to the [Cu_2O_2] plane could also influence the LMCT transition energies, since geometric distortions that reduce the overlap of the amine nitrogen σ-donor orbitals with the primarily Cu(III) d_{xy} LUMO should lower the energy of the latter relative to the oxygen-based donors. Although it is difficult to confirm whether the ∼8° dihedral core twist observed in the crystal structure of [**3b**·$4CH_2Cl_2$] persists in solution, any such distortion arising from the chirality of the CD backbone is likely operative to a similar degree in all of **1b**−**4b**. Notably, samples of **4b** exhibit the same LMCT absorption maxima whether they are prepared from racemic ($_{rac}\mathbf{L}^{\mathbf{TE}}$) or enantiomerically pure ($_{RR}\mathbf{L}^{\mathbf{TE}}$) ligand, implying that spontaneous chiral self-sorting takes place, that both ligands induce similar twists, or that whatever degree of N−Cu−N twisting distortion does persist in solution has negligible effect on the LMCT energy. The lupin alkaloid (−)-sparteine, a rigid bicyclic amine that enforces a pronounced tetrahedral distortion of the Cu centers in its bis(μ-hydroxo)dicopper(II) dimer,[25] forms an **O** that exhibits relatively low-energy LMCT transitions (330, 427 nm). It is not known whether this relative bathochromic shift is due to an analogous twisting distortion, an increased Cu···Cu separation mandated by similar steric concerns, or the larger chelate bite angle (at parity of Cu−N distances) that differentiates (−)-sparteine from the CD, ED, and [9]ane ligand families employed in this work.

(93) Jacobson, R. R.; Tyeklár, Z.; Farooq, A.; Karlin, K. D.; Liu, S.; Zubieta, J. *J. Am. Chem. Soc.* **1988**, *110*, 3690−3692.
(94) Lee, S. C.; Holm, R. H. *J. Am. Chem. Soc.* **1993**, *115*, 11789−11798.
(95) Kau, L. S.; Spira-Solomon, D. J.; Penner-Hahn, J. E.; Hodgson, K. O.; Solomon, E. I. *J. Am. Chem. Soc.* **1987**, *109*, 6433−6442.
(96) Solomon, E. I.; Tuczek, F.; Root, D. E.; Brown, C. A. *Chem. Rev.* **1994**, *94*, 827−856.

Scheme 4. Presumed General Mechanism for the Formation of **O**s

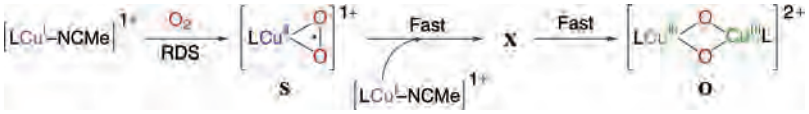

Scheme 5. Proposed Mechanism of Formation for **4b**

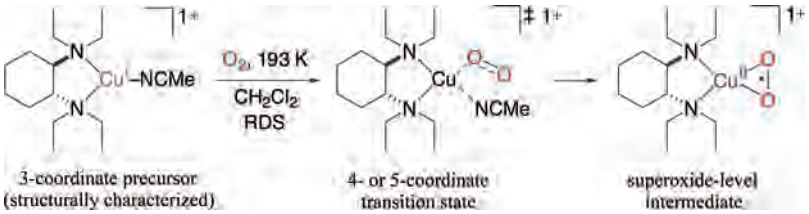

Although ligand-modulated changes in solvation and ion-pairing that create an altered dielectric environment at the **O** core cannot be entirely ruled out as an additional influence on the observed LMCT energies, inspection of a representative sampling of **1b**−**7b** synthesized in various solvents (THF, CH_2Cl_2, acetone) and with various weakly coordinating counteranions ($CF_3SO_3^-$, ClO_4^-, SbF_6^-) suggests that such factors are subordinate to ligand identity in this regard.[40]

Formation Mechanism. Among the **O**s studied, only the formation of **4b** in O_2-saturated CH_2Cl_2 or mixtures thereof occurs slowly enough to facilitate monitoring by conventional mixing techniques under the conditions employed (1 atm O_2, 193 K). The reaction is first-order in [**4a**] (i.e., rate = k_{obs}[**4a**]) and is presumed to be second-order overall (i.e., $k_{obs} = k[O_2]$). This finding is consistent with the general mechanism originally proposed for self-assembled Cu−O_2 species by Zuberbühler,[98,99] which involves initial formation of a mononuclear $[LCu(O_2)]^{1+}$ species (**S**, Scheme 4) in the rate-determining step (RDS), followed by rapid reaction with a second equivalent of the Cu(I) precursor to generate a binuclear "peroxide-level" intermediate (**X**, Scheme 4).[100] Similar first-order formation kinetics have been reported for **O**s based on the mononucleating $\mathbf{L}^{\mathbf{iPr_3TACN}}$ and dinucleating $\mathbf{L}^{\mathbf{iPr_4dtne}}$ ligands.[17,44] Neither **S** nor **X** is observable spectroscopically in these cases because fast subsequent steps preclude their accumulation. However, such 1:1 intermediates—which may be formally described as either superoxocopper(II) or peroxocopper(III) species—have been observed spectroscopically as both transient[10,98,101−110] and stable species[74,111−113] in other Cu−O_2 systems that employ sufficiently bulky ligands. Two structurally characterized examples of charge-neutral $[LCu(O_2)]$ complexes also exist;[15,32,74] one of these reacts anaerobically with sterically compact Cu(I) and Ni(I) species to generate nonsymmetric mixed-ligand **O**s[32] and a heterobimetallic bis(μ-oxo)copper(III)nickel(III) complex,[114] respectively.

The substantial disparity between the formation rates of **4b** ($t_{1/2} \approx 1600$ s) and **1b**−**3b** ($t_{1/2} \leq 5$ s) in CH_2Cl_2 is intriguing. We suggest that the large *N*-alkyl substituent steric effect on the rate of **O** formation ($k_{\mathbf{1b-3b}}/k_{\mathbf{4b}} \geq 300$; CH_2Cl_2, 193 K) arises from an increase in coordination number upon addition of O_2 during the RDS, from 3-coordinate Cu(I) to 4-coordinate or possibly 5-coordinate Cu(II) in the transition state (Scheme 5), consistent with the strongly negative value of $\Delta S^{\ddagger} = -210(40)$ J K^{-1} mol^{-1}/−50(10) cal K^{-1} mol^{-1} measured upon oxygenation of **4a** in 1:1 (v/v) THF/CH_2Cl_2. Given the poor donor capability of the O_2 molecule prior to efficient electron transfer[115] and the comparatively strong Cu−MeCN interaction evidenced by short (∼1.86 Å) Cu−$N_{nitrile}$ bonds in the crystal structures of **4a** and **10a** (vide supra), this associative model offers a more energetically reasonable description of the O_2 binding step than does

(97) Orbital symmetries and bonding/antibonding designations are given relative to a hypothetical O−O bond vector.[66]
(98) Karlin, K. D.; Wei, N.; Jung, B.; Kaderli, S.; Zuberbühler, A. D. *J. Am. Chem. Soc.* **1991**, *113*, 5868−5870.
(99) Zuberbühler, A. D. In *Bioinorganic Chemistry of Copper*; Karlin, K. D., Tyeklár, Z., Eds.; Chapman and Hall: New York, 1993.
(100) It is possible that intermediate **X** (Scheme 3) represents a multistep sequence involving different peroxide-level Cu(II) intermediates, not all of which are bona fide **P** species.
(101) Karlin, K. D.; Wei, N.; Jung, B.; Kaderli, S.; Niklaus, P.; Zuberbühler, A. D. *J. Am. Chem. Soc.* **1993**, *115*, 9506−9514.
(102) Lee, D.-H.; Wei, N.; Murthy, N. N.; Tyeklár, Z.; Karlin, K. D.; Kaderli, S.; Jung, B.; Zuberbühler, A. D. *J. Am. Chem. Soc.* **1995**, *117*, 12498−12513.
(103) Karlin, K. D.; Lee, D. H.; Kaderli, S.; Zuberbühler, A. D. *Chem. Commun.* **1997**, 475−476.
(104) Becker, M.; Heinemann, F. W.; Schindler, S. *Chem. Eur. J.* **1999**, *5*, 3124−3129.
(105) Schatz, M.; Becker, M.; Walter, O.; Liehr, G.; Schindler, S. *Inorg. Chim. Acta* **2001**, *324*, 173−179.
(106) Comba, P.; Kerscher, M.; Merz, M.; Müller, V.; Pritzkow, H.; Remenyi, R.; Schiek, W.; Xiong, Y. *Chem. Eur. J.* **2002**, *8*, 5750−5760.
(107) Weitzer, M.; Schatz, M.; Hampel, F.; Heinemann, F. W.; Schindler, S. *J. Chem. Soc., Dalton Trans.* **2002**, *5*, 686−694.
(108) Schatz, M.; Leibold, M.; Foxon, S. P.; Weitzer, M.; Heinemann, F. W.; Hampel, F.; Walter, O.; Schindler, S. *Dalton Trans.* **2003**, 1480−1487.
(109) Zhang, C.; Kaderli, S.; Costas, M.; Kim, E.; Neuhold, Y.; Karlin, K.; Zuberbühler, A. D. *Inorg. Chem.* **2003**, *42*, 1807−1824.
(110) Weitzer, M.; Schindler, S.; Brehm, G.; Schneider, S.; Hormann, E.; Jung, B.; Kaderli, S.; Zuberbühler, A. D. *Inorg. Chem.* **2003**, *42*, 1800−1806.
(111) Chen, P.; Root, D. E.; Campochiaro, C.; Fujisawa, K.; Solomon, E. I. *J. Am. Chem. Soc.* **2003**, *125*, 466−474.
(112) Schatz, M.; Raab, V.; Foxon, S. P.; Brehm, G.; Schneider, S.; Reiher, M.; Holthausen, M. C.; Sundermeyer, J.; Schindler, S. *Angew. Chem., Int. Ed.* **2004**, *43*, 4360−4363.
(113) Komiyama, K.; Furutachi, H.; Nagatomo, S.; Hashimoto, A.; Hayashi, H.; Fujinami, S.; Suzuki, M.; Kitagawa, T. *Bull. Chem. Soc. Jpn.* **2004**, *77*, 59−72.
(114) Aboelella, N. W.; York, J. T.; Reynolds, A. M.; Fujita, K.; Kinsinger, C. R.; Cramer, C. J.; Riordan, C. G.; Tolman, W. B. *Chem. Commun.* **2004**, 1716−1717.
(115) Given that cyclic voltammograms of the Cu(I) complexes **1a**−**4a** and **10a** in anaerobic CH_2Cl_2 each exhibit a quasi-reversible oxidation wave with $E = 0.9-1.2$ V vs SCE, we contend that outer-sphere electron transfer from Cu(I) to O_2 is not a practicable initial step in the **O** formation mechanism.

dissociative MeCN substitution, which would require a nonlinear, thermodynamically unfavorable, 2-coordinate Cu(I) intermediate. Bulkier *N*-alkyl substituents should inhibit associative expansion of the coordination sphere, resulting in slower oxygenation rates.

Consistent with this mechanism, the most sterically demanding CD-based Cu(I) complex examined, **10a**, does not form an optically detectable $Cu-O_2$ species at 193 K, and it appears to be air-stable even at ambient temperature. Its ostensible O_2 inertness cannot be a kinetic phenomenon, since the auxiliary MeCN ligand undergoes rapid exchange on the NMR time scale and is readily displaced by $CO_{(g)}$. Space-filling molecular modeling based on the crystal structure of [**10a**·$2CH_2Cl_2$] indicates sufficient space for associative substitution of the MeCN ligand by a dioxygen molecule, even in a "side-on" η^2 orientation. The failure to observe spectroscopic features attributable to a 1:1 Cu/O_2 adduct suggests that formation of such an intermediate is thermodynamically unfavorable relative to **10a** and O_2. It is important to note, however, that even significant equilibrium concentrations of a transient Cu(II)−superoxide species could remain undetectable via optical spectroscopy: a recent spectroscopic study of $[Cu(O_2)\{\mathbf{L}^{\mathbf{HB(3-Ad-5-}i\mathbf{Prpz)_3}}\}]$ (Ad = 1-adamantyl) revealed no molar absorptivities greater than 400 M^{-1} cm^{-1} over the entirety of the UV−vis and NIR regions.[111] If a 1:1 intermediate does form upon reaction of **10a** with O_2, it may be prevented from further aggregation by interligand steric interference due to interlocking edge-to-face π-stacking interactions between the four forward-projecting *N*-benzyl substituents (Figure 2). The strong upfield shift of the doublet resonance ($\delta = 6.55$) corresponding to the relevant ortho aryl protons in the ^{1}H NMR spectrum of **10a** suggests that this π-stacked conformer persists in solution.

The observed formation rate of **4b** varies dramatically with solvent choice. At 193 K and 1 atm O_2 pressure, oxygenation of **4a** proceeds at least 300 times faster in THF or acetone than in CH_2Cl_2—that is, at a rate indistinguishable from the lower bound documented for **1b**−**3b** via conventional mixing techniques. The greater relative solubility of O_2 in THF or acetone,[43,116] while certainly a contributing factor, is insufficient in magnitude to account for such a large discrepancy in rates. As an inner-sphere process,[115] O_2 activation at Cu is greatly dependent upon the accessibility of the metal ion. The observed solvent effect may thus be attributed reasonably to subtle differences in ligand conformation, solvent association, or ion-pairing proclivity that modulate the accessibility of the metal.

Reactivity. Toward exogenous substrates the **O** core exhibits a pattern of reactivity (Scheme 2) best characterized as that of a mild $2e^-$ oxidant, often acting via sequential $1e^-$ hydrogen atom abstractions. The characteristic intense LMCT bands of **1b**−**5b** are fully quenched by spectrophotometric titration with 2 equiv of either $Me_{10}Fc$ ($E_{1/2} = -100$ mV vs SCE)[117] or Fc (480 mV)[117,118] but are unaffected by AcFc (750 mV) within 6 h at 193 K. All of the **O**s surveyed were capable of oxidizing alkyl and aryl thiols to the corresponding disulfides and DBP to a coupled biaryl in near-quantitative yields at 193 K under N_2—a net $2e^-$, $2H^+$ process. Noncoordinating hydrocarbon substrates with weak C−H bonds are not appreciably oxidized by any of **1b**−**7b** at 193 K under the conditions employed in this study, although such reactivity has recently been documented for certain **O**s[28] and **O**-containing isomeric mixtures,[18,119] as well as for other anionically stabilized Cu(III) complexes.[120]

Os **1b**−**7b** are limited in their reactivity toward alcohols. The oxidatively susceptible benzyl and cinnamyl alcohols are converted stoichiometrically to the corresponding conjugated aldehydes only when first activated by deprotonation, and saturated primary alcohols are unreactive even when converted to lithium alkoxide salts. In our report of $[(\mathbf{L}^{\mathbf{TMPD}})_2Cu_2(\mu\text{-}O)_2](CF_3SO_3)_2$, a similar **O** that does oxidize primary alcohols directly at 233 K, we attributed the enhanced reactivity to structural and electronic differences: the weak anionic axial association indicated by EXAFS connotes more facile substrate access to the $[Cu_2O_2]^{2+}$ core relative to the **O**s reported in this study.[22] Altered geometry due to increased chelate ring size (i.e., a six-membered chelate for $\mathbf{L}^{\mathbf{TMPD}}$ vs a five-membered chelate for CD-, ED-, and [9]ane-based **O**s) may also be a contributing factor: in electrochemical studies,[81,121,122] distortions from ideal square-planar coordination geometry have been shown to increase the potential of the Cu(III/II) couple.

Kinetic Aspects of Thermal Decomposition. Although stable at low temperatures, **O**s **1b**−**9b** decompose upon warming through a mechanism primarily involving oxygenation of the ligand, as previously described for **1b**, **3b**, **4b**, and **8b**,[21] as well as other **O**s.[2] The thermal decomposition of each **O** (Scheme 6) is fitted readily to a first-order kinetic model and entails $2e^-$—and sometimes $4e^-$—oxidation of an *N*-alkyl pendant group. Our interest in decomposition studies was motivated by broad disparities in thermal sensitivity and ligand product distribution among these structurally homologous **O**s, which are distinguished solely by the nature of their *N*-alkyl substituents. For example, at 263 K, **1b** is ∼20 times more thermally stable than **3b** and ∼170 times more thermally stable than **4b**. Notably, the thermal decay process appears comparatively uninfluenced by solvent and counteranion effects, as is evidenced by the equivalent values of $\Delta H^{\ddagger}$ and $\Delta S^{\ddagger}$ obtained from Eyring fits for the decay of [**5b**·$(CF_3SO_3)_2$] in THF and CH_2Cl_2 and for [**5b**·$(CF_3SO_3)_2$] and [**5b**·$(SbF_6)_2$] in THF.[59]

(116) Jung, B.; Karlin, K. D.; Zuberbühler, A. D. *J. Am. Chem. Soc.* **1996**, *118*, 3763−3764.
(117) Connelly, N. G.; Geiger, W. E. *Chem. Rev.* **1996**, *96*, 877−910.
(118) Chang, D.; Malinski, T.; Ulman, A.; Kadish, K. *Inorg. Chem.* **1984**, *23*, 817−824.
(119) The report by Karlin et al. of such reactivity at −80 °C (*J. Am. Chem. Soc.* **1998**, *120*, 12960−12961) has been reevaluated. See Shearer, J.; Xin Zhang, C.; Zakharov, L. N.; Rheingold, A. L.; Karlin, K. D. *J. Am. Chem. Soc.* **2005**, *127*, 5469−5483.
(120) Lockwood, M. A.; Blubaugh, T. J.; Collier, A. M.; Lovell, S.; Mayer, J. M. *Angew. Chem., Int. Ed.* **1999**, *38*, 225−227.
(121) Hanss, J.; Beckmann, A.; Krüger, H.-J. *Eur. J. Inorg. Chem.* **1999**, 163−172.
(122) Ribas, X.; Jackson, D. A.; Donnadieu, B.; Mahia, J.; Parella, T.; Xifra, R.; Hedman, B.; Hodgson, K. O.; Llobet, A.; Stack, T. D. P. *Angew. Chem., Int. Ed.* **2002**, *41*, 2991−2994.

Scheme 6. Proposed Unimolecular (2e⁻) and Bimolecular (4e⁻) Decomposition Pathways (CD-Based **O**s Shown)

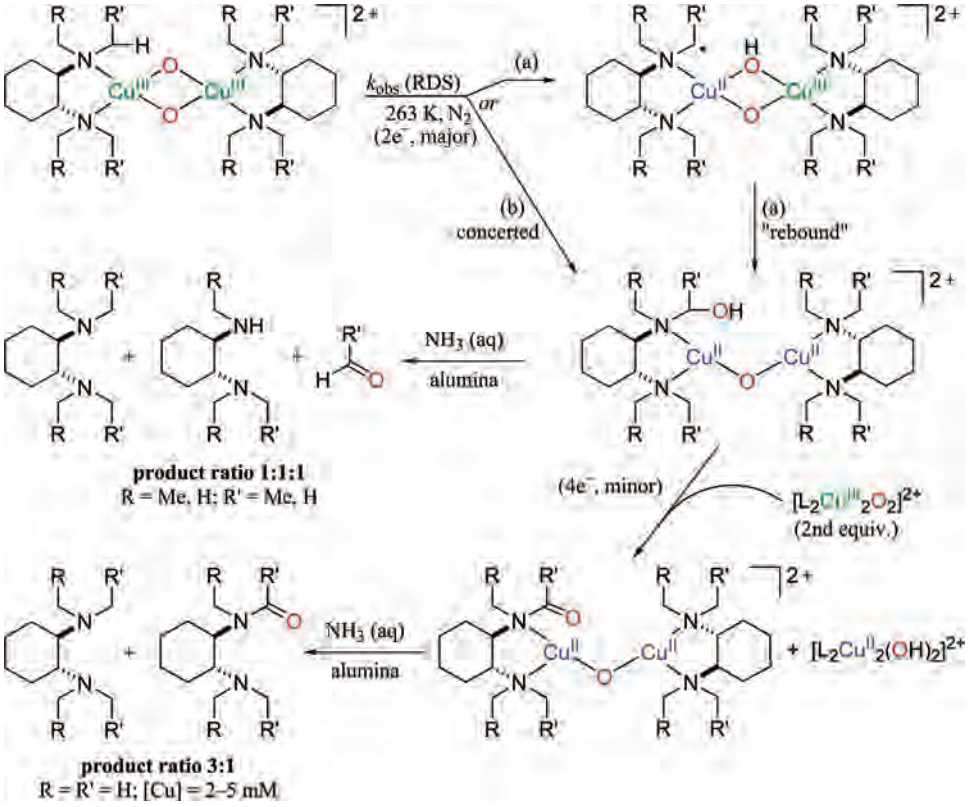

Scheme 7. Selectivity during Thermal Decay of **3b**

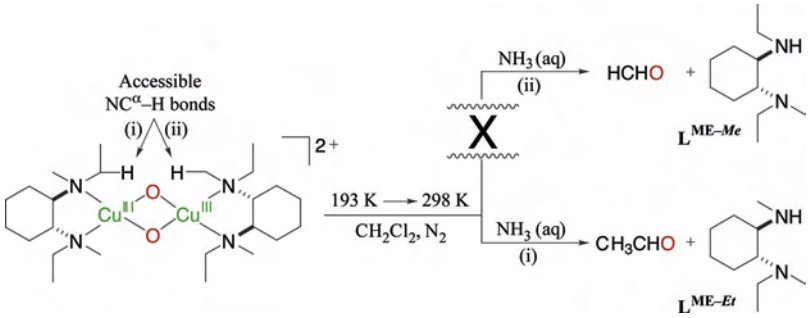

KIE studies were undertaken in order to investigate the thermal decay process further. The comparison of **1b** with d_{24}-**1b** presents a straightforward and informative picture of the thermal decay process, as both **O**s give rise to analogous ligand products that imply a common decomposition pathway. The observed primary KIE of $k_{obs}{}^{H}/k_{obs}{}^{D} \approx 8$ for this reaction at 293 K[123] is in accord with the classically predicted value of ~6.5.[124] This observation provides evidence for cleavage of a methyl C−H bond during the RDS (Scheme 6). By contrast, selective deuteration of the methylene units of the *N*-ethyl substituents in **3b** yields an extrapolated primary KIE of $k_{obs}{}^{H}/k_{obs}{}^{D} \approx 3$ at 293 K. Ligand product analyses (vide infra) offer a plausible explanation for the apparent attenuation of the KIE relative to **1b**: whereas h_8-**3b** generates only the de-ethylated ($\mathbf{L}^{\mathbf{ME}-Et}$) product upon thermal decomposition and workup, d_8-**3b** yields both de-ethylated (d_4-$\mathbf{L}^{\mathbf{ME}-Et}$) and de-methylated ($d_4$-$\mathbf{L}^{\mathbf{ME}-Me}$) products in a ~1:1 ratio (Scheme 7). The NCα−D bond dissociation energy (BDE) in d_8-**3b** is sufficiently elevated relative to h_8-**3b** to activate a competitive decay pathway involving rate-limiting oxidation of a *N*-methyl group.

Rate-determining NCα−H bond activation is the norm among other reported **O**s, some of which exhibit much larger, nonclassical KIEs attributed to quantum-mechanical proton tunneling.[24,45] C−H bond cleavage could theoretically proceed via hydride transfer; however, on the basis of Hammett studies of **O**s derived from tridentate ligands incorporating para-substituted *N*-benzyl groups, the hydride model has generally been rejected in favor of either a hydrogen abstraction or a nonsynchronous concerted mechanism (Scheme 6, paths (a) and (b), respectively).[2,24,45,133] In the case of **1b** and **3b**, the ~2-fold decrease of the thermal decomposition rate in the presence of O_2 (1 atm) suggests involvement of radical species.

The nature of the *N*-alkyl substituents dramatically affects the thermal stability of **O**s: at ambient temperature, decom-

(123) The primary KIE for the thermal decay of **1b**/d_{24}-**1b** might be even larger, since only a 40% yield (i.e., 80% theoretical) of the $\mathbf{L}^{\mathbf{TM}-Me}$ product is observed.

(124) Lowry, T. H.; Richardson, K. S. *Mechanism and Theory in Organic Chemistry*, 3rd ed.; HarperCollins: New York, 1987.

position half-lives ($t_{1/2}$) for the reported compounds span almost 3 orders of magnitude (d_{24}-**1b**, $t_{1/2}$ = 1600 s; **4b**, extrapolated $t_{1/2} \approx 2$ s; 293 K). The observed 20-fold difference in decay rates between **1b** and **3b** (Table 3) is predominantly attributable to the disparity in their activation enthalpies: $\Delta\Delta H^{\ddagger}_{\mathbf{1b-3b}} = 7$ kJ mol^{-1}/1.8 kcal mol^{-1}; $\Delta\Delta S^{\ddagger}_{\mathbf{1b-3b}} = -3$ J K^{-1} mol^{-1}/-0.8 cal K^{-1} mol^{-1}. This corresponds well with the 1.9 kcal mol^{-1} difference in the reported molar NC$^{\alpha}$−H BDEs of trimethylamine (92.6 ± 1 kcal mol^{-1}) and triethylamine (90.7 ± 0.4 kcal mol^{-1}).[125] By contrast, the 8-fold difference between the decay rates of **3b** and **4b** arises almost exclusively from the entropic terms: $\Delta\Delta H^{\ddagger}_{\mathbf{3b-4b}} = -0.5$ kJ mol^{-1}/-0.1 kcal mol^{-1}; $\Delta\Delta S^{\ddagger}_{\mathbf{3b-4b}} = -21$ J K^{-1} mol^{-1}/-5 cal K^{-1} mol^{-1}. The negligible $\Delta\Delta H^{\ddagger}$ is consistent with a mechanism in which both **3b** and **4b** decompose solely via NC$^{\alpha}$−H bond cleavage of *N*-ethyl substituents having equivalent BDEs; as already noted, ligand degradation product analysis confirms that the *N*-ethyl substituent is indeed selectively oxidized in the case of **3b**. The significant disparity in activation entropy terms may reflect the 2-fold relative increase in the number of accessible *N*-ethyl groups, as well as greater preorganization of these substituents owing to increased steric congestion about the **O** core in **4b**.

Comparison of Eyring plots[59] for the thermal decomposition of **O**s based on the permethylated facial-capping tridentate ligands $\mathbf{L^{Me_3TACN}}$ and $\mathbf{L^{Me_2ODACN}}$ (**8b** and **9b**, respectively) gives insight into the effect of ligand denticity—more specifically, the presence or absence of axial donors—on thermal stability. The superior thermal robustness of **9b** derives mainly from enthalpic considerations that may reflect the substantially weaker donor strength of the axially bonded ether oxygen atom of $\mathbf{L^{Me_2ODACN}}$ ($\Delta\Delta H^{\ddagger}_{\mathbf{9b-8b}} = 9.0$ kJ mol^{-1}/2.2 kcal mol^{-1}; $\Delta\Delta S^{\ddagger}_{\mathbf{9b-8b}} = -12$ J K^{-1} mol^{-1}/-2 cal K^{-1} mol^{-1}). The [N_2O] donor set in $\mathbf{L^{Me_2ODACN}}$ generates an **O** that is more thermally stable than its [N_3] $\mathbf{L^{Me_3TACN}}$ analogue by an order of magnitude, suggesting that the stronger axial σ donation in the latter destabilizes its **O** core. Indeed, **1b**, which lacks an integral axial ligand donor altogether, enjoys a 100-fold advantage in thermal stability over **8b**, at parity of *N*-alkyl substituents (viz. methyl). Coordination of axial ligands is known to increase the reduction potential of Cu(III) complexes generally,[79,120] although the particular comparison of **1b** with [9]ane-based **O**s is complicated by the fluxional axial−equatorial ligand exchange documented for some members of the latter family.[16] That the disparity in activation entropies ($\Delta\Delta S^{\ddagger}_{\mathbf{1b-8b}} = -24$ J K^{-1} mol^{-1}/-6 cal K^{-1} mol^{-1}) is counterstatistical with regard to the number of available methyl hydrogens tends to support the relevance of other factors. The large quantum tunneling-induced primary KIEs observed in some [9]ane-based systems[45] also suggest a fundamentally different juxtaposition of *N*-alkyl substituents to the $[Cu_2O_2]^{2+}$ core.

Ligand Degradation Product Analysis. The observed distribution of *N*-dealkylated ligand products within the CD and ED series (Table 3) is consistent with the general mechanism outlined in Scheme 6. In several instances, however, the observed yields of such products are insufficient to account for all oxidizing equivalents on a 2e$^-$/**O** basis. For example, upon decomposition and workup, **1b** and **3b** generate the $\mathbf{L^{TM-}}^{Me}$ and $\mathbf{L^{ME-}}^{Et}$ products in 60% and 80% of theoretical yields, respectively, whereas **4b** produces the $\mathbf{L^{TE-}}^{Et}$ product in near-quantitative (>95%) yield. Yields of $\mathbf{L^{X-}}^{R}$ products for the ED-based **O**s **5b**−**7b** are likewise substantially substoichiometric despite excellent (>90%) ligand mass recovery during analysis. These reproducible observations raise the prospect of a competing exogenous reductant, although comparative thermal decomposition studies conducted in deuterated solvents have revealed no significant solvent KIE, and no other decay products were detected by GC-MS or ^{1}H NMR analysis. The fate of the remaining oxidizing equivalents is currently under investigation.

The appearance of a 4e$^-$ oxidized formamide $\mathbf{L^{TM+}}^{O}$ product in up to 20% theoretical yield at higher concentrations of **1b** ([Cu] = 2−5 mM, 263 K, THF) strongly suggests the involvement of an aminol intermediate (Scheme 6), subsequent oxidation of which leads to the formamide product.[126] Analogous 4e$^-$-oxidized species are the major ligand products in the thermal decomposition of the [9]ane-based **O**s **8b** and **9b**, and similar products have been reported for other [9]ane systems.[52] As proposed by Itoh and Tolman,[24,45] the rate-limiting oxygen atom insertion into the NC$^{\alpha}$−H bond generates an aminol intermediate. This unstable species, the major ligand product in the chiefly unimolecular decay of CD- and ED-based **O**s, converts to the dealkylated $\mathbf{L^{X-R}}$ end product upon workup, the detached *N*-alkyl substituent having been oxidized to the corresponding aldehyde. The formamide product is proposed to arise from intermolecular overoxidation of the aminol intermediate by a second equivalent of **O** in a bimolecular process that becomes significant at higher concentrations of **1b** and predominates generally in the cases of **8b** and **9b**. Evidence for such a process—formally, a net oxygen atom transfer from the Cu_2O_2 core to the ligand—has been given previously via $^{18}O_2$ labeling studies in which the label was transferred from $[(\mathbf{L^{Bn_3TACN}})_2Cu_2(\mu\text{-}^{18}O)_2]^{2+}$ to the carbonyl product.[45]

C−H Bond Cleavage. The selectivity of intraligand C−H bond cleavage in **O**s depends on the nature of the *N*-alkyl ligand substituents and the degree to which they are physically accessible to the $[Cu_2O_2]^{2+}$ core. A comparison of the ligand products from the decay of **3b** and **6b** underscores the importance of *N*-alkyl group positioning as well as NC$^{\alpha}$−H BDE in steering the thermal decomposition process: whereas **3b** generates exclusively $\mathbf{L^{ME-}}^{Et}$, **6b** yields both $\mathbf{L^{(MeEt)_2ED-}}^{Et}$ and $\mathbf{L^{(MeEt)_2ED-}}^{Me}$ products in comparable quantities but at a much lower combined yield (25% of theoretical vs 80% for **3b**). The absence of selectivity in the latter case is attributed to the increased conformational freedom of the ED ligand backbone, which affords the *N*-methyl groups more competitive access to the **O** core. The marked difference in decay rates between ED- and CD-based

(125) Dombrowski, G. W. D., J. P.; Farid, S.; Goodman, J. L.; Gould, I. R. *J. Org. Chem.* **1999**, *64*, 427−431.

(126) No corresponding 4e$^-$-oxidized product was detected for the thermal decomposition of **3b** at Cu concentrations up to 50 mM.

Os is likewise consistent with this analysis: at 263 K, **6b** decays 8 times more slowly than the more rigid **3b** because the greater backbone flexibility of the former allows the *N*-alkyl substituents to occupy a wider range of positions less conducive to $NC^{\alpha}-H$ bond cleavage. Similarly, **4b** decays ~5 times faster than **5b** despite a larger entropic barrier attributable to its relatively more constrained transition state [$\Delta\Delta H^{\ddagger}_{\mathbf{4b-5b}} = 11.0$ kJ mol^{-1}/-2.7 kcal mol^{-1}; $\Delta\Delta S^{\ddagger}_{\mathbf{4b-5b}} = -30$ J K^{-1} mol^{-1}/-7 cal K^{-1} mol^{-1}]. At parity of *N*-alkyl substituents, the comparatively low overall yields of *N*-dealkylated ligand products among the ED-based **O**s are also consistent with the slower observed decay rates, assuming that such substoichiometric yields are due in general to a competing process involving an exogenous reductant (vide supra).

The importance of core accessibility at parity of backbone structure is further exemplified by comparison of the isomeric ED-based **O**s **6b** and **7b**. Whereas the former yields a mixture of ligand products (vide supra), the latter decays 20 times faster and generates the $\mathbf{L^{Me_2Et_2ED-}}$*Et* product exclusively. The $\mathbf{L^{(MeEt)_2ED}}$ ligand in **6b** can achieve greater conformational flexibility by virtue of the symmetric distribution of its bulk throughout the complex; hence, both *N*-ethyl and *N*-methyl groups are susceptible to oxidation. By contrast, the conformational freedom of the nonsymmetric $\mathbf{L^{Me_2Et_2ED}}$ ligand in **7b** is limited by steric congestion of its geminal *N*-ethyl substituents, which may be thus constrained to positions more accessible to the $[Cu_2O_2]^{2+}$ core. These steric considerations, in conjunction with the 1.9 kcal mol^{-1} disparity in BDE between *N*-methyl and *N*-methylene C−H bonds, are sufficient to produce the observed selectivity.

Upon inspection of the crystal structure of [**3b**·4CH_2Cl_2], it is possible to make similar inferences regarding the importance of core accessibility in the thermal decay of **3b**. In explaining its dealkylation selectivity, one might assign equal relevance to both the disparity in $NC^{\alpha}-H$ BDEs and the steric constraints imposed on the *N*-ethyl substituents by the rigid $\mathbf{L^{ME}}$ ligand backbone. In the solid state, at least, the four inward-directed methylene hydrogens of these *N*-ethyl groups participate in C−H···O hydrogen bonding interactions that place them as little as 2.45 Å away from the bridging oxides and as close as 0.62 Å to the $[Cu_2O_2]$ least-squares plane (C−H bond lengths fixed to 1.1 Å). Since the LUMO + 1 orbital that is presumed to be the main acceptor MO for the $NC^{\alpha}-H$ bond cleavage process is a predominantly metal-based combination of the in-plane Cu d_{xy} and oxygen σ^* orbitals,[45,66,127] C−H bonds that approach coplanarity with the $[Cu_2O_2]$ rhomb should achieve better overlap with this orbital, and thus exhibit greater susceptibility to $NC^{\alpha}-H$ bond cleavage. Moreover, space-filling molecular models of the [**3b**·4CH_2Cl_2] crystal structure suggest that the geared configuration of the *N*-alkyl substituents restricts free rotation of the *N*-ethyl groups about the C−N bond, effectively locking them into an orientation that is conducive to $NC^{\alpha}-H$ bond cleavage. The *N*-methyl hydrogens, by comparison, are at least 2.29 Å distant from the $[Cu_2O_2]$ least-squares plane in the solid state, and they possess a much greater degree of rotational freedom that should further reduce their exposure to the core.

Although the crystal structure of [**3b**·4CH_2Cl_2] certainly provides insight into the types of ligand−core interactions that may influence the $NC^{\alpha}-H$ bond cleavage mechanism, the limitations of such parallels between solid-state structural data and the behavior of solution species become evident in considering the thermal decay of d_8-**3b**. In this case, attack of the $\mathbf{L^{ME}}$ *N*-methyl substituents becomes competitive with de-ethylation merely upon selective deuteration of the *N*-methylene units, implying that relative differences in C−H(D) BDE exert the deciding influence in this system. More generally, this surprising result suggests that it is in fact a complex interplay of factors including relative $NC^{\alpha}-H$ BDEs, thermally induced vibrational distortions, sterically imposed constraints on ligand substituent conformations, and statistical factors that governs the ligand product selectivity observed in each particular instance.

Conclusions

We have synthesized and characterized a family of simple vicinal PDL−Cu(I) precursors and their corresponding thermally labile **O**s, as well as related tridentate **O**s based on the [9]ane skeleton. The essential spectroscopic features of these **O**s are consistent over a large number of peralkylated di- and triamine ligands, and include intense LMCT bands at ~300 and ~400 nm, an intense O_2 isotope-sensitive band in the rR spectrum at ~600 cm^{-1} ($\Delta\nu(^{16}O_2-^{18}O_2) \approx 25$ cm^{-1}), characteristically short Cu−O (~1.80 Å) and Cu···Cu (~2.75 Å) distances, and an XAS edge profile typical of trivalent Cu. The well-ordered crystal structure of [**3b**·4CH_2Cl_2] provides one of the most metrically compact examples of an **O** core yet reported—a result we ascribe to the minimization of intramolecular steric interactions. The square-planar geometry and bridging dianionic oxide ligands in the $[Cu_2(\mu\text{-}O)_2]^{2+}$ core provide a highly stabilizing coordination environment for Cu(III). The mechanism of formation of these **O**s is best described as rate-determining generation of a Cu(II)−superoxide species followed by reaction with another molecule of the Cu(I) precursor; the rate of formation may be influenced by ligand steric factors as well as solvent effects.

The chemical reactivity profile of **O**s is that of a mild oxidant that reacts with suitable exogenous substrates, or with its own ligands through a $NC^{\alpha}-H$ bond cleavage mechanism. Careful analysis of the dealkylated ligand decay products provides further support for the proposed mechanism and suggests that the relative thermal stabilities of the reported **O**s are dictated not solely by the strength of ligand substituent $NC^{\alpha}-H$ bonds but also by their position and degree of conformational freedom relative to the $[Cu_2O_2]^{2+}$ core. This latter attribute is, in turn, very much dependent on ligand geometry and conformational rigidity. The same factors also have a marked effect on the internal selectivity of ligand oxidation during thermal decay, as ligand substituents that have weak $NC^{\alpha}-H$ bonds constrained in a comparatively

(127) Pidcock, E.; Obias, H. V.; Zhang, C. X.; Karlin, K. D.; Solomon, E. I. *J. Am. Chem. Soc.* **1998**, *120*, 7841−7847.

favorable position relative to the **O** core are preferentially attacked. **O**s based on bidentate ligands lack the destabilizing influence of an axial σ donor for Cu(III), and so possess greater thermal stability at parity of *N*-alkyl substituents than those based on comparable tridentate ligands. With a half-life of almost 30 min at 293 K, the perdeuterated d_{24}-**1b** is the most thermally stable dicationic **O** species currently known.

That a bidentate ligand with the most compact *N*-alkyl substituents (methyl) provides the greatest thermal stability is as fortunate as it is fortuitous, for it preserves a potential for reactivity with exogenous organic substrates that is determined primarily by accessibility to the **O** core. Although the products are not yet known, the observation of sub-stoichiometric yields of dealkylated ligands in the case of more thermally stable **O**s such as **1b** and **6b** is encouraging insofar as a portion of their reactivity is directed outward toward substrates or solvent rather than inward toward the ligands. Achieving such exogenous reactivity at biologically relevant temperatures remains a primary goal in ligand design.

Experimental Section

Materials. CH_2Cl_2 obtained from Fisher Scientific was stirred over concentrated H_2SO_4 for several days, washed thoroughly with several portions of 1 M KOH, and then washed with deionized H_2O until clear. After fast drying with either $K_2CO_{3(s)}$ or $CaCl_{2(s)}$, it was allowed to stand for several days over $P_4O_{10(s)}$ in the absence of light and O_2, and was subsequently distilled under like conditions and stored in a N_2 drybox. THF and diethyl ether (Et_2O) were obtained from Fisher Scientific and distilled under N_2 from the corresponding solution of the Na−benzophenone ketyl radical. Spectrophotometric-grade MeCN was obtained from Fisher Scientific. Spectrophotometic-grade acetone was distilled from $K_2CO_{3(s)}$. NaH was obtained as a 60% mineral oil dispersion (Aldrich), washed repeatedly with dry hexane in a N_2 drybox, dried in vacuo, and stored under N_2. Salts $[Cu(MeCN)_4](X)$, where $X^- = CF_3SO_3^-$, ClO_4^-, or SbF_6^-, were synthesized from Cu_2O (Aldrich) and HX (Aldrich) by a variation of the literature method.[128] Prior to use, they were recrystallized twice from MeCN/Et_2O and stored under dry N_2. Ferrocene, acetylferrocene, and decamethylferrocene were obtained from Aldrich and either recrystallized or sublimed before use. *trans*-(1*R*,2*R*)-Cyclohexanediamine (CD) was resolved as the tartrate salt from a commercially available diamine mixture (DuPont DCH-99) according to the method of Whitney.[87] The racemic form, (±)-*trans*-1,2-cyclohexanediamine ($_{rac}$CD), was separated as the oxalate salt from the same commercial mixture in an analogous procedure. All diamine ligands except $\mathbf{L^{TB}}$ were purified by flash distillation in vacuo from $CaH_{2(s)}$ or $NaH_{(s)}$ and stored in a N_2 drybox.

Methods. Preparation and manipulation of air-sensitive Cu complexes were carried out using standard Schlenk techniques or in a N_2 drybox (M. Braun). Since many of the Cu(I) complexes tended to decompose to yellowish, insoluble products on standing in CH_2Cl_2 solution, these compounds were generally prepared in situ. Low-temperature UV−vis spectra were obtained using a Polytec PI X-DAP-06 spectrophotometer in conjunction with a custom-designed immersible quartz fiber-optic probe (Hellma, Inc.) with a variable optical path length (0.01, 0.1, and 1.0 cm) and custom air-free sample cells (ChemGlass). X-ray crystal data were collected on Enraf-Nonius CAD4 and Bruker-Siemens SMART diffractometers and were refined using teXsan 1.04 and CrystalStructure 2.0 from Molecular Structure Corp., as well as the SHELX-97 routine of George Sheldrick. The refined models were checked and evaluated using PLATON for Windows;[129] ORTEP figures were generated via Ortep-3 for Windows[130] and POV-ray 3.5 for Windows. ^{1}H and ^{13}C NMR spectra (including low-temperature magnetic susceptibility measurements)[65] were performed on a Varian XL 400 MHz instrument. The derived molar susceptibilities were corrected for the diamagnetic contributions of the ligands and solvent, which were estimated using Pascal's constants.[131] Gas chromatography/mass spectrometry (GC-MS) was performed on an HP 5970 gas chromatograph with an in-line MS detector, using an AT-5 (Alltech) column. Ligand purity was assessed on an HP 5890 gas chromatograph with an HP-DB1 column and an FID detector. Multivariate analysis of UV−vis kinetic data was performed using SPECFIT.[132] Cyclic voltammograms of Cu(I) species were recorded at a scan rate of 100 mV s^{-1} on a CV-50W voltammetric analyzer from Bioanalytical Systems using a Pt wire counter electrode, a Pt button working electrode, and a $Ag/AgCl_{(s)}$ reference electrode; conditions were as follows: 1.0 mM analyte concentration, N_2 atmosphere, CH_2Cl_2 solvent, 0.1 M tetra-*n*-butylammonium perchlorate supporting electrolyte. Solution FTIR spectra were collected on an ATI Mattson Infinity Series spectrophotometer using an air-free CaF_2 liquid flow cell. Elemental analyses were performed by Desert Analytics (Tucson, AZ); samples were dried under vacuum overnight prior to analysis and handled anaerobically.

Syntheses of Ligands. *trans*-(1*R*,2*R*)-Cyclohexanediamine (CD) and (±)-*trans*-1,2-Cyclohexanediamine ($_{rac}$CD). Enantiopure CD tartrate (25 g, 99 mmol) or an equivalent amount of $_{rac}$CD oxalate was dissolved in the minimum amount of 10 M KOH. KOH pellets (20 g) and Et_2O (500 mL) were added, and the mixture was stirred vigorously for 24 h. The resulting solution was decanted, and the solid residue was pulverized and washed with 50 mL portions of Et_2O. To minimize the formation of insoluble carbonate salts, exposure to atmospheric moisture and CO_2 was limited by appropriate use of N_2 blanketing. The solvent was removed from the combined organic phases in vacuo at 293 K, and the residue was distilled in vacuo from $CaH_{2(s)}$ to yield 8.9 g of the free base (80%). ^{1}H NMR ($CDCl_3$, 400 MHz): δ 1.05−1.2 (m, 2H); 1.25−1.35 (br m, 6H); 1.7 (m, 2H); 1.85 (d, 2H); 2.25 (m, 2H).

***N,N,N′,N′*-Tetramethyl-*trans*-(1*R*,2*R*)-cyclohexanediamine ($\mathbf{L^{TM}}$).**[56] CD (3.0 g, 26.3 mmol) was added to 2.4 g of HCOOH (52.6 mmol) and 4.2 g of HCHO (37% aqueous solution, 52.6 mmol) and the mixture refluxed for 24 h. The solution was cooled to 298 K, made basic with 2 M aqueous NaOH, and extracted with Et_2O (4 × 25 mL). The resulting solution was dried over $K_2CO_{3(s)}$ and the solvent removed by rotary evaporation. The resulting brown oil was distilled in vacuo from $CaH_{2(s)}$ to give 3.1 g of a colorless oil (70%). $_{rac}\mathbf{L^{TM}}$ was prepared from $_{rac}$CD in an identical manner. ^{1}H NMR ($CDCl_3$, 400 MHz): δ 1.0−1.2 (m, 4H); 1.7 (m, 2H); 1.77 (m, 2H); 2.23 (m, 12H); 2.55 (m, 2H). GC-MS: *m*/*z* 170, M^+.

(128) Kubas, G. J.; Monzyk, B.; Crumbliss, A. L. *Inorg. Synth.* **1979**, *19*, 90−92.
(129) Spek, A. *J. Appl. Crystallogr.* **2003**, *36*, 7−13.
(130) Farrugia, L. J. *J. Appl. Crystallogr.* **1997**, *30*, 565.
(131) Drago, R. S. *Physical Methods for Chemists*, 2nd ed.; Saunders: Orlando, FL, 1992.
(132) Binstead, R.; Zuberbühler, A. Spectrum Software Associates, Marlborough, MA.
(133) Spuhler, P.; Holthausen, M. C. *Angew. Chem., Int. Ed.* **2003**, *42*, 5961−5965.

***d*$_{12}$-*N*,*N*,*N*′,*N*′-Tetramethyl-*trans*-(1*R*,2*R*)-cyclohexanediamine (*d*$_{12}$-L^{TM}).** The perdeutero-*N*-methyl analogue of **L^{TM}** was prepared as above from CD (0.470 g, 4.12 mmol) using d_2-formic acid (2.06 g, 41.2 mmol) and d_2-formaldehyde (20% aqueous solution in D_2O, 1.32 g, 41.2 mmol). Yield 50%. ^{1}H NMR ($CDCl_3$, 400 MHz): δ 1.0−1.2 (m, 4H); 1.7 (m, 2H); 1.77 (m, 2H); 2.55 (m, 2H). GC-MS: *m*/*z* 182, M^+.

***N*,*N*′-Diacetyl-*trans*-(1*R*,2*R*)-cyclohexanediamine.** CD (3.5 g, 31.3 mmol) was refluxed with a large excess of acetic anhydride (100 mL) in dry toluene ($PhCH_3$, 100 mL) for 4 h with stirring. The white crystals of the *N*,*N*′-diacetyl derivative that formed on cooling to 273 K were filtered, washed with successive 10 mL portions of cold $PhCH_3$ and Et_2O, and recrystallized from 1:1 (v/v) $PhCH_3/Et_2O$ (4.5 g, 75%). ^{1}H NMR ($CDCl_3$, 400 MHz): δ 1.28 (br m, 4H); 1.75 (m, 2H); 1.95 (s, 6H); 2.05 (m, 2H); 3.65 (m, 2H); 6.1 (br s, 2H).

***N*,*N*′-Diethyl-*trans*-(1*R*,2*R*)-cyclohexanediamine.** *N*,*N*′-diacetyl-*trans*-(1*R*,2*R*)-cyclohexanediamine (4.5 g, 23.0 mmol) was suspended in 250 mL of dry, freshly distilled, deoxygenated THF and cooled to 273 K on an ice bath. To this mixture were added 120 mL of 1.0 M BH_3 in THF via cannula. After the addition was complete, the reaction mixture was warmed to 293 K, heated at reflux 3 h with stirring under N_2, and finally acidified by cautious addition of excess 4 M aqueous HCl (50 mL) and refluxed for an additional 1 h. The resulting mixture was concentrated to a volume of ∼50 mL by boiling, made basic (pH > 12) by cautious addition of 10 M KOH at 273 K, and extracted with Et_2O (6 × 25 mL). The combined organic fractions were dried over $K_2CO_{3(s)}$ and concentrated on a rotary evaporator, yielding an oily residue (3.5 g, 90%). The crude diamine product was subjected to methylation directly.

***d*$_4$-*N*,*N*′-Diethyl-*trans*-(1*R*,2*R*)-cyclohexanediamine.** A suspension of *N*,*N*′-diacetyl-*trans*-(1*R*,2*R*)-cyclohexanediamine (0.700 g, 3.54 mmol) in 200 mL of dry, deoxygenated THF was cooled to 273 K. $LiAlD_4$ (Aldrich, 0.150 g, 36 mmol) was added cautiously under N_2, and the mixture was stirred for 15 min with attendant warming and vigorous effervescence. The reaction mixture was heated at reflux with stirring under a N_2 atmosphere for 12 h and then cooled to 298 K, after which the excess $LiAlD_4$ was quenched via cautious addition of MeOH. The solvent was removed in vacuo and the residue treated with excess 10 M KOH. The mixture was then extracted with Et_2O (4 × 25 mL), and the combined organic fractions were dried over $K_2CO_{3(s)}$. The solvent was again removed by rotary evaporation, leaving an oily residue of the crude diamine (0.400 g, 70%), which was subjected to methylation directly.

***N*,*N*′-Diethyl-*N*,*N*′-dimethyl-*trans*-(1*R*,2*R*)-cyclohexanediamine (L^{ME}) and *d*$_4$-*N*,*N*′-Diethyl-*N*,*N*′-dimethyl-*trans*-(1*R*,2*R*)-cyclohexanediamine (*d*$_4$-L^{ME}).** Methylation of crude *N*,*N*′-diethyl-*trans*-(1*R*,2*R*)-cyclohexanediamine and *d*$_4$-*N*,*N*′-diethyl-*trans*-(1*R*,2*R*)-cyclohexanediamine was performed as described for **L^{TM}**, with yields of ∼70% in each case. **L^{ME}**: ^{1}H NMR ($CDCl_3$, 400 MHz): δ 1.05 (t, 6H); 1.05−1.20 (br m, 4H); 1.65−1.80 (m, 4H); 2.23 (s, 6H); 2.55 (q + m, 6H). GC-MS: *m*/*z* 198, M^+. *d*$_4$-**L^{ME}**: ^{1}H NMR ($CDCl_3$, 400 MHz): δ 1.05 (t, 6H); 1.05−1.20 (br m, 4H); 1.65−1.80 (m, 4H); 2.23 (s, 6H); 2.55 (q, 2H). GC-MS: *m*/*z* 202, M^+.

3-Acetyl-1,3-thiazolidine-2-thione. Triethylamine (30 g, 296 mmol) was added to a solution of 2-mercaptothiazoline (20.0 g, 168 mmol) in 400 mL of CH_2Cl_2. Acetyl chloride (15.8 g, 201 mmol) was added gradually with stirring, and the clear yellow solution which resulted was then washed with successive 100-mL portions of 10% aqueous HCl and 1 M aqueous NaOH, dried over $K_2CO_{3(s)}$, and concentrated to an oil by rotary evaporation. Upon standing in a freezer for several days at 253 K, the oil slowly crystallized (14.2 g, 50%). ^{1}H NMR ($CDCl_3$, 400 MHz): δ 2.78 (s, 3H); 3.29 (t, 2H); 4.58 (t, 2H).

***N*-Acetyl-*trans*-(1*R*,2*R*)-cyclohexanediamine.** A solution of 3-acetyl-1,3-thiazolidine-2-thione (7.2 g, 45 mmol) in 50 mL of CH_2Cl_2 was added dropwise over the course of 1 h to a solution of CD (5.0 g, 44 mmol) in CH_2Cl_2 (150 mL). The resulting bright red solution was extracted with aqueous acetate buffer (1 M NaOAc, 2 M HOAc, 3 × 50 mL). The combined aqueous fractions were washed with CH_2Cl_2 (3 × 50 mL, washings discarded), made basic (pH > 12) by addition of saturated aqueous KOH, and extracted with CH_2Cl_2 (5 × 50 mL). Drying the combined organic fractions over $K_2CO_{3(s)}$ and removing the solvent in vacuo yielded 4.8 g of solid product, which was contaminated with significant amounts of unreacted CD starting material, as well as the diacetylated byproduct. The crude solid was then purified, first by heating to 373 K under a dynamic vacuum for several hours to remove the more volatile CD (600 mg recovered) and thereafter by sublimation in an open Pyrex tube at 473 K. The white, microcrystalline product was resublimed once in the same manner (3.7 g, 55%). ^{1}H NMR ($CDCl_3$, 400 MHz): δ 1.1−1.4 (br m, 4H); 1.75 (m, 4H); 1.95 (s, 3H); 2.02 (m, 3H); 3.63 (m, 1H); 5.89 (br s, 1H).

***N*-Ethyl-*trans*-(1*R*,2*R*)-cyclohexanediamine.** *N*-Acetyl-*trans*-(1*R*,2*R*)-cyclohexanediamine (3.7 g, 23.7 mmol) was suspended in 300 mL of dry, freshly distilled, deoxygenated THF and cooled to 273 K in an ice bath. To this mixture were added 100 mL of 1 M BH_3 in THF via cannula. After refluxing for 3 h with stirring under N_2, the solution was acidified by cautious addition of 4 M aqueous HCl (150 mL) and refluxed for an additional 1 h. The mixture was then concentrated to a volume of 50 mL by boiling. The concentrate was made basic (pH > 12) by cautious addition of KOH pellets, diluted with sufficient H_2O to dissolve precipitated salts, and extracted with Et_2O (6 × 25 mL). The combined organic fractions were dried over $K_2CO_{3(s)}$ and concentrated on a rotary evaporator, yielding an oily, partially crystalline residue (4 g) which was employed in further steps without characterization.

***N*-Ethyl-*N*,*N*′,*N*′-trimethyl-*trans*-(1*R*,2*R*)-cyclohexanediamine (L^{EtMe_3}).** Crude *N*-ethyl-*trans*-(1*R*,2*R*)-cyclohexanediamine was permethylated and purified in the manner described for **L^{TM}** (3.5 g colorless oil, 19 mmol, 43% overall yield). ^{1}H NMR ($CDCl_3$, 400 MHz): δ 1.07 (t, 3H); 1.02−1.21 (br m, 4H); 1.65−1.93 (br m, 4H); 2.20 (s, 3H); 2.30 (m, 6H); 2.40−2.60 (br m, 2H); 2.52 (q, 2H). GC-MS: 353 K (1 min), 30 K min^{-1} to 473 K (10 min); t_R = 9.7 min (*m*/*z* 184, M^+).

***N*,*N*,*N*′,*N*′-Tetraethyl-*trans*-(1*R*,2*R*)-cyclohexanediamine (L^{TE}).** CD (3.10 g, 27.7 mmol) and $NaH_{(s)}$ (10 g) were suspended in dry $PhCH_3$ (150 mL), and the resulting slurry was refluxed under N_2. Excess diethyl sulfate (30 mL) was added slowly by syringe, and the mixture was refluxed for 24 h. Residual hydride was quenched by cautious addition of MeOH (50 mL), after which the mixture was poured into 1.0 L of a 1 M aqueous NaOH solution and extracted with Et_2O (4 × 50 mL). The combined organic layers were dried over $K_2CO_{3(s)}$ and the solvent removed by rotary evaporation. The brown, oily residue was distilled in vacuo from $CaH_{2(s)}$ to give 3.5 g of a clear oil (60%). $_{rac}$**L^{TE}** was prepared in an identical manner from $_{rac}$CD. ^{1}H NMR ($CDCl_3$, 400 MHz): δ 1.01 (t, 12H); 1.05−1.20 (m, 4H); 1.64−1.70 (m, 2H); 1.76−1.84 (m, 2H); 2.40−2.50 (sextet, 4H); 2.56−2.68 (m, 6H). GC-MS: *m*/*z* 226, M^+.

***N*,*N*′-Diethyl-*N*,*N*′-dimethyl-1,2-ethanediamine (L$^{(MeEt)_2ED}$).** *N*,*N*′-Diethyl-1,2-ethanediamine (Aldrich) was permethylated and purified as described for **L^{TM}** (80%). ^{1}H NMR ($CDCl_3$, 400 MHz): δ 1.01 (t, 4H); 1.9 (s, 6H); 2.0−2.2 (m, 10H). GC-MS: *m*/*z* 144, M^+.

***N*,*N*-Diethyl-*N*′,*N*′-dimethyl-1,2-ethanediamine (L^{Me_2Et_2ED}).** *N*,*N*-Diethyl-1,2-ethanediamine (Aldrich) was permethylated and purified

as described for $\mathbf{L^{TM}}$ (80%). ^{1}H NMR (d_6-acetone, 400 MHz): δ 0.70 (t, 6H); 1.8 (s, 6H); 2.00−2.07 (m, 2H); 2.18−2.25 (q+m, 6H). GC-MS: *m*/*z* 144, M^+.

***N,N,N′,N′*-Tetraethyl-1,2-ethanediamine ($\mathbf{L^{TEED}}$).** $\mathbf{L^{TEED}}$ (Aldrich) was distilled from $CaH_{2(s)}$ before use. ^{1}H NMR ($CDCl_3$, 400 MHz): δ 1.01 (t, 12H); 2.5 (d, 4H); 2.45−2.55 (m, 8H). GC-MS: *m*/*z* 172, M^+.

1,4,7-Trimethyl-1,4,7-triazacyclononane ($\mathbf{L^{Me_3TACN}}$). $\mathbf{L^{Me_3TACN}}$ was synthesized according to the literature method.[54] ^{1}H NMR ($CDCl_3$, 400 MHz): δ 2.4 (s, 9H); 2.7−2.8 (m, 12H). GC-MS: 353 K (1 min), 40 K min^{-1} to 393 K (10 min); t_R = 9.3 min (*m*/*z* 171, M^+).

4,7-Dimethyl-4,7-diaza-1-oxacyclononane ($\mathbf{L^{Me_2ODACN}}$). 4,7-Diaza-1-oxacyclononane (1.1 g, 8.5 mmol), synthesized by the literature method,[55] was permethylated and purified as described for $\mathbf{L^{TM}}$ (0.67 g, 50%). ^{1}H NMR ($CDCl_3$, 400 MHz): δ 2.40 (s, 6H); 2.68 (m, 8H); 3.70 (t, 4H). GC-MS: *m*/*z* 158, M^+.

***N,N,N′,N′*-Tetrabenzyl-*trans*-(1*R*,2*R*)-cyclohexanediamine ($\mathbf{L^{TB}}$).** Freshly distilled CD (2.0 g, 175 mmol) was dissolved in 50 mL of dry, deoxygenated DMF. Finely powdered $K_2CO_{3(s)}$ (12.1 g, 875 mmol) and $PhCH_2Br$ (12.3 g, 700 mmol) were added, and the resulting effervescent milky suspension was stirred 24 h in an oil bath at 353 K under a N_2 atmosphere. The mixture was treated with 100 mL of CH_2Cl_2 and washed with 1 M aqueous NaOH (8 × 100 mL). The organic layer was dried over $K_2CO_{3(s)}$ and the solvent removed in vacuo. The resulting pale oil was redissolved in 20 mL of absolute EtOH and chilled over dry ice until crystallization ensued. The resulting white solid was filtered, washed with cold (193 K) EtOH (3 × 10 mL), and dried in vacuo (2.9 g, 35%). ^{1}H NMR (400 MHz, $CDCl_3$): δ 0.95−1.15 (m, 4H); 1.7 (m, 2H); 2.1 (m, 2H); 2.7 (m, 2H); 3.35 (d, 4H); 3.75 (d, 4H); 7.2−7.3 (m, 12H); 7.4−7.45 (m, 8H). ^{13}C NMR (400 MHz, $CDCl_3$): δ 24.9, 25.9, 53.2, 58.1, 126.5, 127.9, 128.9, 140.6. FAB-MS: *m*/*z* 475.2, M^+.

Syntheses and in situ Preparations of $[LCu(MeCN)]CF_3SO_3$ Complexes 1a−9a (General Procedure). To a solution of $[Cu(MeCN)_4]CF_3SO_3$ (38 mg, 0.10 mmol) in the appropriate amount of CH_2Cl_2, THF, or acetone was added 0.10 mmol of the ligand L, yielding solutions of **1a**−**9a**. **1a**: ^{1}H NMR (CD_2Cl_2, 400 MHz): δ 1.05−1.10 (m, 2H); 1.10−1.25 (br m, 2H); 1.70−1.80 (d, 2H); 1.90−1.98 (d, 2H); 2.19 (CH_3CN, s, 12H); 2.23 (s, 6H); 2.30−2.40 (br m, 2H); 2.49 (s, 6H). **2a**: ^{1}H NMR (CD_2Cl_2, 400 MHz): δ 1.10−1.20 (br m, 2H); 1.20−1.35 (t + br m, 5H); 1.65−1.75 (m, 2H); 1.90−2.00 (br m, 2H); 2.09 (CH_3CN, s, 12H); 2.31 (s, 3H); 2.32 (s, 3H); 2.48−2.51 (br m, 2H); 2.60 (s, 3H); 2.55−2.65 (br m, 1H); 2.60−2.70 (br m, 1H). **3a**: ^{1}H NMR (CD_2Cl_2, 400 MHz): δ 1.05−1.15 (m, 2H); 1.20−1.35 (m, 8H); 1.65−1.75 (m, 2H); 1.90−2.00 (m, 2H); 2.05 (CH_3CN, s, 12H); 2.27 (s, 6H); 2.55−2.80 (br m, 6H). **4a**: ^{1}H NMR (CD_2Cl_2, 400 MHz): δ 1.05−1.15 (br m, 2H); 1.20−1.35 (br m, 14H); 1.75−1.85 (br m, 2H); 1.95−2.05 (br m, 2H); 2.07 (CH_3CN, s, 12H); 2.35 (sextet, 2H); 2.55−2.70 (br m, 6H); 2.91 (sextet, 2H). **5a** ^{1}H NMR (CD_2Cl_2, 300 MHz): δ 1.15−1.19 (t, 12H); 2.08 (CH_3CN, s, 12H); 2.62 (s, 4H); 2.68−2.75 (q, 8H). **6a** ^{1}H NMR (CD_2Cl_2, 300 MHz): δ 1.18−1.13 (t, 6H); 2.08 (CH_3CN, s, 12H); 2.34 (br s, 6H); 2.3−2.9 (br m, 8H). **7a** ^{1}H NMR (CD_2Cl_2, 200 MHz): δ 1.08−1.15 (t, 6H); 2.07 (CH_3CN, s, 12H); 2.44 (s, 6H); 2.45−2.65 (m, 4H); 2.66−2.77 (q, 4H). **8a** ^{1}H NMR (CD_2Cl_2, 500 MHz): δ 2.03 (CH_3CN, s, 12H); 2.68 (s, 4H); 2.69 (br m, 8H). Single diffraction-quality crystals (colorless needles) of **4a** were obtained upon layering a concentrated (50 mM, 2.0 mL) CH_2Cl_2 solution with Et_2O (22 mg, 0.046 mmol, 45%).

$[(_{RR}\mathbf{L^{TM}})_2Cu]CF_3SO_3\cdot[(_{SS}\mathbf{L^{TM}})_2Cu]CF_3SO_3$ (1c). To a solution of $[Cu(MeCN)_4]CF_3SO_3$ (188 mg, 0.50 mmol) in 2 mL of CH_2Cl_2 was added $_{rac}\mathbf{L^{TM}}$ (170 mg, 1.00 mmol). The resulting clear solution was layered with Et_2O and allowed to stand for several days, whereupon large crystals (colorless rectangular blocks) of **1c** slowly formed (195 mg, 35 mmol, 70%). Since **1c** dissociates (with appearance of free ligand resonances) in those NMR solvents in which it dissolves (d_6-DMSO, CD_3CN), no ^{1}H NMR spectrum was obtained.

$[(\mathbf{L^{TM}})Cu(PPh_3)]CF_3SO_3$ (1d). To a solution of $[Cu(MeCN)_4]CF_3SO_3$ (188 mg, 0.50 mmol) in 2 mL of CH_2Cl_2 were added $\mathbf{L^{TM}}$ (85 mg, 0.50 mmol) and PPh_3 (131 mg, 0.50 mmol). The resulting clear solution was layered with cyclohexane and allowed to stand for several days, whereupon large crystals (colorless rhombic blocks) of **1d** slowly formed (270 mg, 0.43 mmol, 85%). ^{1}H NMR ($CDCl_3$): δ 1.10−1.20 (m, 2H); 1.20−1.30 (br m, 2H); 1.75−1.85 (d, 2H); 1.93−1.99 (d, 2H), 2.41 (s, 6H); 2.60 (s, 6H); 2.65−2.70 (br m, 2H).

$[(\mathbf{L^{TB}})Cu(MeCN)]CF_3SO_3$ (10a). $\mathbf{L^{TB}}$ (50 mg, 0.110 mmol) and $[Cu(MeCN)_4]CF_3SO_3$ (40 mg, 0.11 mmol) were dissolved in 1 mL of CH_2Cl_2. Dropwise addition of Et_2O caused the formation of fine white needles of **10a**, which were collected by suction filtration, washed with Et_2O, and dried in vacuo (75 mg, 0.099 mmol, 90%). ^{1}H NMR (400 MHz, $CDCl_3$): δ 1.30−1.40 (m, 2H); 1.45−1.60 (m, 2H); 2.00−2.10 (m, 2H); 2.15 (s, 3H); 2.40−2.50 (m, 2H); 3.02 (d, 2H); 3.20−3.30 (m, 4H); 3.60 (d, 2H); 3.95 (d, 2H); 6.55 (d, 4H); 7.20−7.50 (m, 16H). ^{13}C NMR (400 MHz, $CDCl_3$): δ 23.3, 25.0, 54.5, 56.1, 58.7, 128.6, 128.9, 129.3, 129.5, 131.2, 131.7, 134.5, 135.3. FTIR: $\nu_{C\equiv N}$, 2292 cm^{-1}.

$[(\mathbf{L^{TB}})Cu(CO)]CF_3SO_3$. A solution of [**10a**·$2CH_2Cl_2$] (100 mg, 0.123 mmol) in $CDCl_3$ (1 mL) was sparged briefly with $CO_{(g)}$ and allowed to stand for 15 min under a CO atmosphere (1.7 atm). Dropwise addition of Et_2O caused the precipitation of a microcrystalline solid product, which was recovered by suction filtration and dried in vacuo (74 mg, 0.117 mmol, 95%). ^{1}H NMR (400 MHz, $CDCl_3$): δ 1.40−1.60 (m, 2H); 1.60−1.80 (m, 2H); 2.00−2.10 (m, 2H); 2.15 (s, 3H); 2.50−2.60 (m, 2H); 3.30 (d, 2H); 3.40−3.55 (m, 4H); 3.90 (d, 2H); 4.05 (d, 2H); 6.25 (d, 4H); 7.15−7.40 and 7.50−7.70 (m, 16H). FTIR (CH_2Cl_2 solution): $\nu_{C\equiv O}$, 2113 cm^{-1}.

Syntheses of Bis(μ-hydroxo)dicopper(II) Complexes $[(_{RR}\mathbf{L^{TM}})_2Cu_2(\mu\text{-}OH)_2](CF_3SO_3)_2$ ($_{RR,RR}$1e**) and $[(_{SS}\mathbf{L^{TM}})(_{RR}\mathbf{L^{TM}})Cu_2(\mu\text{-}OH)_2](CF_3SO_3)_2$ ($_{RR,SS}$**1e**).** Method A ($_{RR,RR}$**1e**): A cold solution of **1b** in CH_2Cl_2 (25 mL, [Cu] = 2.0 mM) was injected with 1.1 mL of a 50 mM CH_2Cl_2 solution of DBP or *tert*-butylthiol (2.2 equiv) at 193 K under a N_2 atmosphere, whereupon the color rapidly changed to violet. The solution was warmed to ambient temperature, concentrated to ∼1 mL in vacuo, and layered with Et_2O. Violet rhombic blocks of $_{RR,RR}$**1e** (19 mg, 90%) separated upon standing. Method B ($_{RR,RR}$**1e** and $_{RR,SS}$**1e**): A CH_2Cl_2 solution of **1a** (10 mL, 30 mM; prepared with $_{RR}\mathbf{L^{TM}}$ or $_{rac}\mathbf{L^{TM}}$ as appropriate) was exposed to the atmosphere in an open flask at room temperature (i.e., in the presence of atmospheric moisture), whereupon a rapid color change to deep blue-violet was observed. The solution was layered with Et_2O and allowed to stand for several days, whereupon violet rhombic blocks of the corresponding bis(μ-hydroxo)dicopper(II) dimer $[L_2Cu_2(\mu\text{-}OH)_2](CF_3SO_3)_2$ separated (72 mg, 0.090 mmol, 60%).

General Preparation of Bis(μ-oxo)dicopper(III) Dimers (Os) $[L_2Cu_2(\mu\text{-}O)_2](CF_3SO_3)_2$ (L = $\mathbf{L^{TM}}$, 1b; L = $\mathbf{L^{EtMe_3}}$, 2b; L = $\mathbf{L^{ME}}$, 3b; L = $\mathbf{L^{TE}}$, 4b; L = $\mathbf{L^{TEED}}$, 5b; L = $\mathbf{L^{(MeEt)_2ED}}$, 6b; L = $\mathbf{L^{Me_2Et_2ED}}$, 7b; L = $\mathbf{L^{Me_3TACN}}$, 8b; L = $\mathbf{L^{Me_2ODACN}}$, 9b) and Manometry. Air-free solutions of **1a**−**9a**, prepared in situ in concentrations ranging from 0.1 to 50 mM[62] in purified CH_2Cl_2, THF, or acetone, were chilled to 193 K in a dry ice/2-propanol bath. Dry O_2 was admitted by bubbling with a fine needle,

whereupon the solutions turned yellow- to red-brown (**1b**−**9b**, respectively). Manometric measurements were performed using a calibrated Schlenk line with a dead volume of ∼100 mL, an open-tube mercury manometer, and a 50 mL Teflon-valved flask. A solution of the Cu(I) precursor (**3a**−**5a**, **7a**: CH_2Cl_2, [Cu] = 40 mM) was thoroughly degassed by freeze−pump−thaw cycles (three) and allowed to react with O_2 at 193 K (1 atm initial pressure) for a minimum of 2 h or until gas uptake ceased (maximum 8 h, **4a**). The cooling apparatus was then removed, and the system was allowed to equilibrate at 293 K to account for solvent vapor pressure effects. The decomposed solutions were immediately resubjected to the same procedure to provide a reference measurement in each case. Under the given conditions, a ∼6 cm difference between the reaction and blank corresponded to a 2:1 (Cu/O_2) uptake ratio. The calculated uptake ratios were as follows. **3a**, 2.0(1):1 (average of three trials); **4a**, 2.2:1; **5a**, 1.9(1):1 (average of four trials); **7a**, 2.1-(1):1 (average of three trials). Single crystals of [**3b**·$4CH_2Cl_2$] suitable for X-ray diffraction study (yellow-brown rhombic blocks) were grown by direct diffusion of Et_2O into a concentrated ([Cu] ≈ 50 mM) CH_2Cl_2 solution at 193 K. Selected crystals were examined by light microscopy and mounted on a goniometer at 193 K using an improvised cold stage.

Thermal Decomposition Kinetics. The thermal decomposition reactions of **1b**−**9b**, as well as deuterated complexes d_{24}-**1b** and d_8-**3b**, were monitored in a custom-designed low-temperature cell in CH_2Cl_2 solution (except where otherwise noted) at the following Cu concentrations: **1b**/d_{24}-**1b**: 0.2, 0.5, 1.0, 2.0 mM; **2b**: 1.0 mM; **3b**/d_8-**3b**: 0.2, 1.0, 2.0 mM; **4b**: 1.0, 2.0 mM (CH_2Cl_2 and THF); **5b**: 1.0, 2.0 mM (CH_2Cl_2 and THF, also SbF_6^- counteranion in THF); **6b**: 1.0, 2.0 mM; **7b**: 1.0, 2.0 mM; **8b**: 0.2, 1.0 mM; **9b**: 0.2, 2.0 mM. The **O**s were formed by injecting 1.0 mL of a concentrated (10×) solution of the corresponding Cu(I) complex (**1a**−**9a**) into 9.0 mL of cold, O_2-saturated solvent (193 K, 1 atm). After complete **O** formation was verified by the stabilization of optical absorbances at the expected values (Table 3), the excess O_2 was removed by vacuum/N_2 purge cycles (four) and the complex was allowed to decay at the desired temperature (213−293 K), which was maintained by a thermostatic cooling bath (FTS Systems, New York). Data collection for decay was started only after the solution had attained the desired temperature as detected by an OMEGA surface temperature probe; approximately 2−3 min were normally required for thermal equilibration. A multiwavelength (280−450 nm) component analysis of the data was performed using SPECFIT to obtain rate constants. Data reduction was performed by singular value decomposition analysis followed by Marquardt minimization to the given model. The number of significant eigenvectors obtained was generally 2 for all data sets, and a first-order A → B reaction model provided a suitable fit to each. Reproducibility of the results was checked in each case by conducting multiple trials (minimum three). The decomposed **O** solutions from kinetic runs were generally subjected to analysis (vide infra) to verify ligand product distribution.

Ligand Decomposition Product Analysis (General Procedure for 1b, 3b−9b). For ligand decomposition product analyses, 10-mL CH_2Cl_2 solutions of **O**s (**1b**, [Cu] = 1.0−2.0 mM, also 2.0−5.0 mM in THF; **3b**−**9b**, [Cu] = 0.2−2.0 mM) were prepared at 193 K, degassed by evacuation and backfilling with N_2 (three cycles), and allowed to decompose at a convenient temperature between 213 and 293 K for several hours until the characteristic **O** LMCT bands had completely disappeared. The vessel was removed from the cooling bath, and aqueous NH_3 (30%) was added dropwise to the still-cold solution with vigorous shaking until the CH_2Cl_2 layer was colorless. The organic layer was passed through a column of neutral activated alumina (Brockmann I, ∼150 mesh, 58 Å) followed by the aqueous layer. The column was rinsed with MeOH (2 mL) and the combined metal-free eluents dried over $K_2CO_{3(s)}$. The solution was concentrated by rotary evaporation to ∼2 mL, and a stoichiometric amount of cinnamaldehyde, acetophenone, anthracene, or benzonitrile was added as an internal GC standard. To avoid aerobic oxidation, atmospheric exposure was minimized throughout the workup process via N_2 blanketing and prompt handling. The ligand products (total ligand mass recovery was generally >90%) were subjected to GC/GC-MS analysis.[59]

Spectrophotometric Titrations and Oxidation of Exogenous Substrates (General Procedure). Deoxygenated (N_2, min. 15 min) **O** solutions (**1b**−**7b**; [Cu] = 1.0 mM; 10 mL CH_2Cl_2; 193 K) were prepared and injected with the following substrates dissolved in dry deoxygenated THF or CH_2Cl_2 (0.5 mL, 2 equiv relative to **O** unless otherwise specified): ethylene (1 atm); 9,10-dihydroanthracene (1−5 equiv); fluorene (1−5 equiv); xanthene (1−5 equiv); cyclohexene (1−5 equiv); 1,4-cyclohexadiene (1−5 equiv); 1-octanol (protonated and Li salt); $PhCH_2OH$ (protonated and Li salt); cinnamyl alcohol (protonated and Li salt); $(CH_3)_2S$ (1−5 equiv); $(CH_3)_2SO$ (1−5 equiv); $PhSCH_3$ (1−5 equiv); *tert*-butylthiol; thiocresol; 2,4-di-*tert*-butylphenol. Lithium salts of the alcohols were generated in situ by stoichiometric addition of *n*-butyllithium to a THF solution. The reaction mixtures were maintained at the desired temperature (generally 193 K) under N_2 until no further optical change was evident (max 6 h). The solutions were then passed through a column of neutral activated alumina (Brockmann I, ∼150 mesh, 58 Å) at 293 K followed by two column volumes of MeOH. After drying over $K_2CO_{3(s)}$, the combined copper-free eluents were subjected to GC/GC-MS analysis. Mass recovery of the products was generally >90% as deduced by addition of an internal calibrant. Substrate oxidation products were identified by their GC retention times (t_R) and molecular ion *m*/*z* (M^+) peaks[59] and were confirmed in some cases by comparison of their ^1H and ^{13}C NMR features with literature values.

Spectrophotometric titrations of **1b**−**5b** (193 K, CH_2Cl_2, [Cu] = 1.0 mM) with Fc, AcFc, and $Me_{10}Fc$ were conducted in a similar manner, with successive injections of 0.1 equiv of aliquots spaced at intervals sufficient to allow equilibration. Additional reactions of **1b**−**5b** with AcFc were attempted under like conditions with no change in optical absorbance noted after 6 h.

Acknowledgment. We thank Drs. Frederick J. Hollander and Allen G. Oliver of the UC Berkeley College of Chemistry X-ray Diffraction Facility (CHEXRAY) for collection of X-ray diffraction data. Funding was provided by NIH GM50730 (T.D.P.S). A.P.C. thanks the National Science Foundation for a predoctoral fellowship, and L.M.M. gratefully acknowledges a John Stauffer Graduate Fellowship.

Supporting Information Available: Characterization of products from ligand decomposition and exogenous substrates oxidation; initial rates plot for the oxygenation of **4a**; Eyring plots and kinetic data for thermal decomposition of **1b**, **3b**, **4b**, **5b**, **8b**, and **9b**; experimental details, atomic positions, anisotropic thermal parameters, bond distances, bond angles, torsional angles, and CIF files for the crystal structures of **1c**, **1d**, $_{RR,SS}$**1e**, $_{RR,RR}$**1e**, **3b**, **4a**, and **10a**; input coordinates for hybrid DFT calculations on homochiral and heterochiral formulations of **1c** (PDF). This material is available free of charge via the Internet at http://pubs.acs.org.

IC050331I